Supporting Information

Nitric Oxide Activation by Distal Redox Modulation in Tetranuclear Iron Nitrosyl Complexes

Graham de Ruiter, Niklas B. Thompson, Davide Lionetti, and Theodor Agapie*

Division of Chemistry and Chemical Engineering, California Institute of Technology, Pasadena, California 91125, United States. Email: agapie@caltech.edu

Table of Contents

Synthetic Procedures

Figures

Tables

Synthesis of [$LFe_3(PhPz)_3OFe$]. In the glovebox, to a rapidly stirred suspension of [$LFe_3OFe(PhPz)_3$][OTf] (100 mg, 0.06 mmol) in THF (3 mL), was added a solution of $CoCp^*_2$ (20 mg, 0.06 mmol) in THF (1 mL). The suspension turned metallic blue immediately and was stirred for an additional 2h. After 2h. the solid was collected on a fine porosity glass frit and washed with 5 mL of THF and 5 mL of MeCN. The remaining solid was collected and dried under vacuum to yield a blue solid (86 mg; 94%).

Synthesis of [$LFe_3(PhPz)_3OFe$][BF_4] from [$LFe_3(PhPz)_3OFe$]. In the glovebox, to a suspension of the proposed [$LFe_3(PhPz)_3OFe$] (60.1 mg, 0.04 mmol) in MeCN (4 mL), was added a solution of $AgBF_4$ (7.6 mg, 0.04 mmol) in MeCN (1mL). Upon addition, the suspension became homogeneous and turned brown. After 2h., the solution was filtered over Celite, and the volatiles removed under reduced pressure to yield $LFe_3(PhPz)_3OFe][BF_4]$ as a red/brown solid. Yield 57 mg (83%) Crystals suitable for X-ray analysis were grown by vapor diffusion of diethyl ether into a concentrated solution of **3** in CH_2Cl_2. ^1H NMR (300 MHz, CD_2Cl_2): identical to that of [$LFe_3(PhPz)_3OFe$][OTf] (Figure S7 and S11). ^{19}F NMR (282 MHz, CD_2Cl_2) δ -153.20.

Synthesis of [$LFe_3(PhPz)_3OFe$][OTf] from [$LFe_3(PhPz)_3OFe$]. In the glovebox, to a suspension of [$LFe_3(PhPz)_3OFe$][OTf] (17 mg; 0.01 mmol) in THF (2 mL), was added a solution $CoCp^*_2$ (3.6 mg, 0.01 mmol) in mL THF (0.5 mL). A blue precipitate formed immediately and the suspension was stirred for 1 h. Next the solvent was removed under reduced pressure and the residue re-suspended in MeCN (2 mL). To the suspension was added a solution of AgOTf (2.7 mg, 0.01 mmol) in MeCN (0.5 mL). The solution turned homogeneous immediately, and turned red/brown. After 2h., the solution was filtered over Celite, and the volatiles removed under reduced pressure to yield $LFe_3(PhPz)_3OFe][OTf]$ as a red/brown solid. ^1H NMR (300 MHz, CD_2Cl_2): identical to that of [$LFe_3(PhPz)_3OFe$][OTf] (Figure S7 and S11)

Addition of $[LFe_3(PhPz)_3OFe(NO)][OTf]$ to $[LFe_3(PhPz)_3OFe(NO)][OTf]_3$. In the glovebox, to a solution of $[LFe_3(PhPz)_3OFe(NO)][OTf]$ (17.8 mg; 0.01 mmol) in CD_2Cl_2 (0.6 mL) was added a solution of $[LFe_3(PhPz)_3OFe(NO)][OTf]_3$ (19.7 mg; 0.01 mmol) in CD_2Cl_2 (0.6 mL). The solution turned green immediately, and was transferred to a J-Young tube, and the ^1H NMR was recorded after 1 hour and 24 hours (Figure S27). Both ^1H NMR spectra are identical to that of $[LFe_3(PhPz)_3OFe(NO)][OTf]_2$ (Figure S18)

Addition 1 atm. O_2 to $[LFe_3(PhPz)_3OFe(NO)][OTf]$. In the glovebox, a solution of $[LFe_3(PhPz)_3OFe(NO)][OTf]$ (17.4 mg; 0.01 mmol) in CD_2Cl_2 (0.6 mL) was added to a J-Young NMR tube and sealed. The solution was degassed on the Schlenk line by three freeze-pump-thaw cycles. While still frozen 1 atm. of O_2 was added to the NMR tube and sealed. The reaction was monitored by ^1H-NMR and spectra were recorded after 30 minutes, 2 hours, and 24 hours (Figure S28). The ^1H NMR spectra after 2 hours is identical to that of $[LFe_3(PhPz)_3OFe(NO)][OTf]_2$ (Figure S18). Hereafter, some decomposition is observed.

Addition 1 atm. O_2 to $[LFe_3(PhPz)_3OFe(NO)][OTf]_3$. In the glovebox, a solution of $[LFe_3(PhPz)_3OFe(NO)][OTf]_3$ (19.4 mg; 0.01 mmol) in CD_2Cl_2 (0.6 mL) was added to a J-Young NMR tube and sealed. The solution was degassed on the Schlenk line by three freeze-pump-thaw cycles. While still frozen 1 atm. of O_2 was added to the NMR tube and sealed. The reaction was monitored by ^1H-NMR and spectra were recorded after 30 minutes, 2 hours, and 24 hours. No changes in the ^1H-NMR were observed during the course of the reaction (Figure S29)

Addition 6 equiv. NO to $[LFe_3(PhPz)_3OFe(NO)][OTf]$. In the glovebox, a 100 mL Schlenk tube was charged with $[LFe_3(PhPz)_3OFe(NO)][OTf]$ (81.1 mg, 0.05 mmol) and acetonitrile (15 mL) was added. The tube was sealed and degassed by three freeze-pump-thaw cycles on the Schlenk-line. While frozen, gaseous nitric oxide (NO, 36.7 mL, 0.0.18998 atm., 144.4 mm Hg)

was added. The mixture was stirred at room temperature for 28 h, during which, the color changed from yellow/brown to green. Hereafter, on the high-vacuum line, all the volatiles were vacuum transferred through a series of traps at -78 ºC (to trap the acetonitrile), and finally to an evacuated 10 mL round-bottom Schlenk-flask maintained at -196 ºC (to trap the remaining gassed; e.g. NO or N2O). After complete transfer of all volatiles, the 10 mL Schlenk-flask was sealed and its gaseous contents transferred to an evacuated IR-cell for analyses (Figure 7). The remaining solid in the 100 mL Schlenk-tube was transferred to the glove-box and dissolved in CH_2Cl_2 (5 mL). The volatiles were removed under reduced pressure to yield a green solid (Yield 100 % by NMR). The ^{1}H NMR is identical to that of $[LFe_3(PhPz)_3OFeNO][OTf]_2$ (Figure S18).

Addition 6 equiv. NO to $[LFe_3(PhPz)_3OFe(NO)][OTf]_3$. In the glovebox, a 100 mL Schlenk tube was charged with $[LFe_3(PhPz)_3OFe(NO)][OTf]_3$ (96.2 mg, 0.05 mmol) and acetonitrile (15 mL) was added. The tube was sealed and degassed by three freeze-pump-thaw cycles on the Schlenk-line. While frozen, gaseous nitric oxide (NO, 36.7 mL, 0.0.18998 atm., 144.4 mm Hg) was added. The mixture was stirred at room temperature for 28 h. No color change was observed during this time period. Hereafter, on the high-vacuum line, all the volatiles were vacuum transferred through a series of traps at -78 ºC (to trap the acetonitrile), and finally to an evacuated 10 mL round-bottom Schlenk-flask maintained at -196 ºC (to trap the remaining gassed; e.g. NO or N2O). After complete transfer of all volatiles, the 10 mL Schlenk-flask was sealed and its gaseous contents transferred to an evacuated IR-cell for analyses (Figure 7). The remaining solid in the 100 mL Schlenk-tube was transferred to the glove-box and dissolved in CH_2Cl_2 (5 mL). The volatiles were removed under reduced pressure to yield a purple/brown solid (Yield 100 % by NMR). The ^{1}H NMR is identical to that of $[LFe_3(PhPz)_3OFeNO][OTf]_3$ (Figure S19).

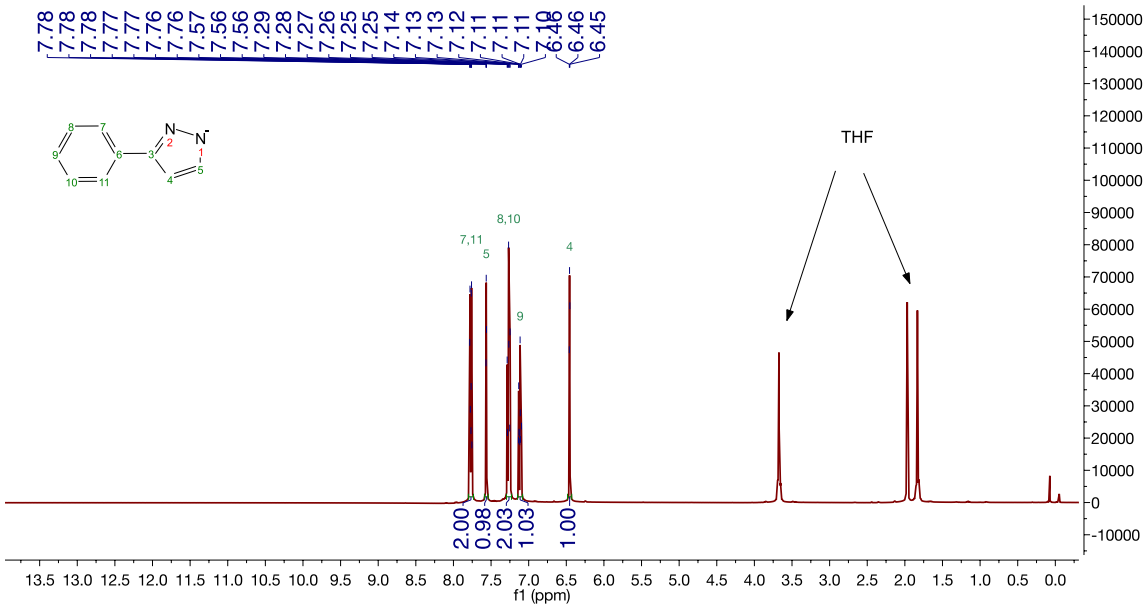

Figure S1. ^{1}H NMR spectrum (400 MHz) of NaPhPz in CD_3CN.

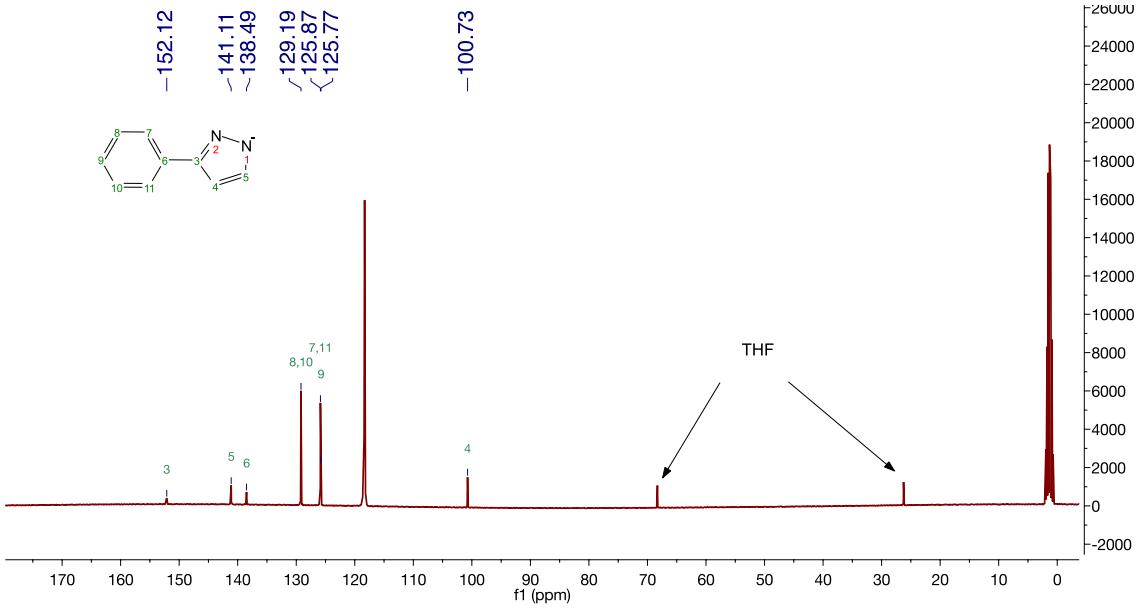

Figure S2. ^{13}C NMR spectrum (100 MHz) of NaPhPz in CD_3CN.

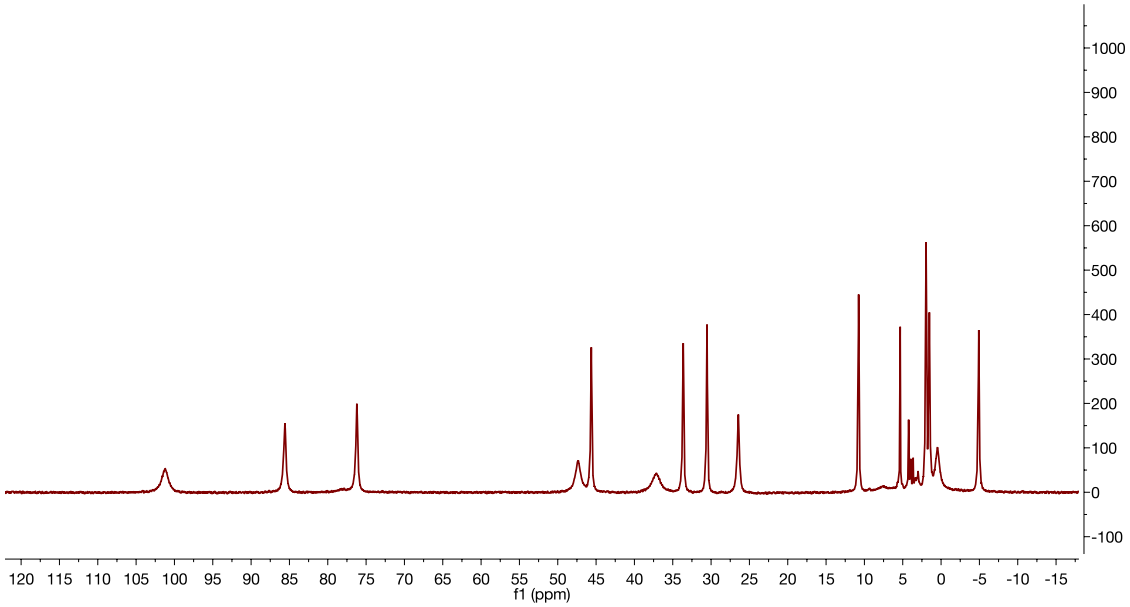

Figure S3. ^{1}H NMR spectrum (300 MHz) of $LFe_3(OAc)(OTf)_2$ in CD_2Cl_2.

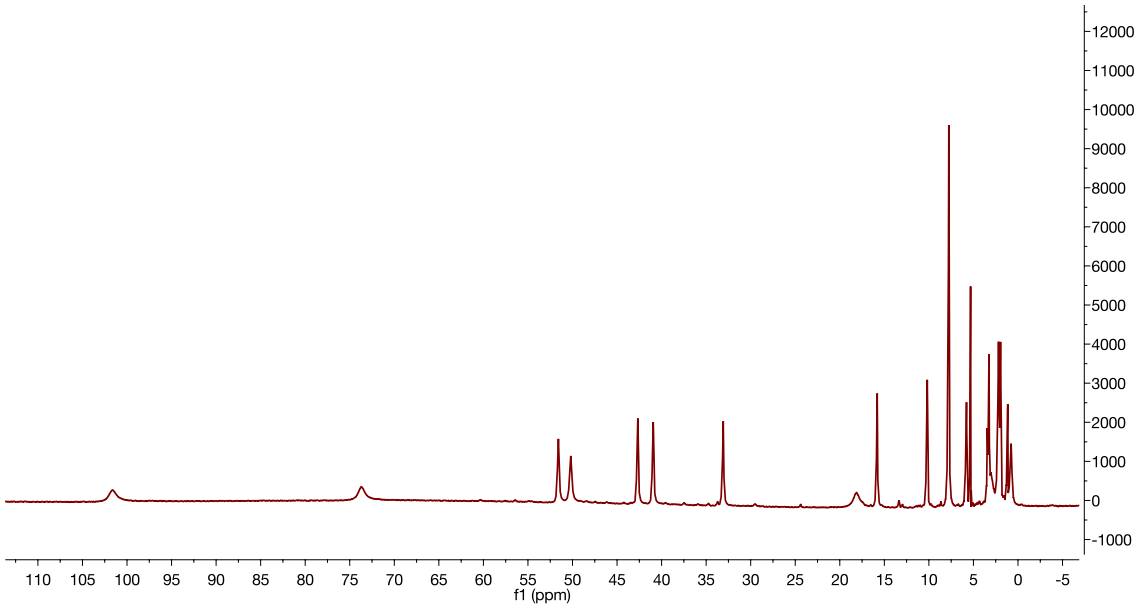

Figure S4. ^{1}H NMR spectrum (300 MHz) of $[LFe_3(PhPz)_3ONa][OTf]$ in CD_2Cl_2.

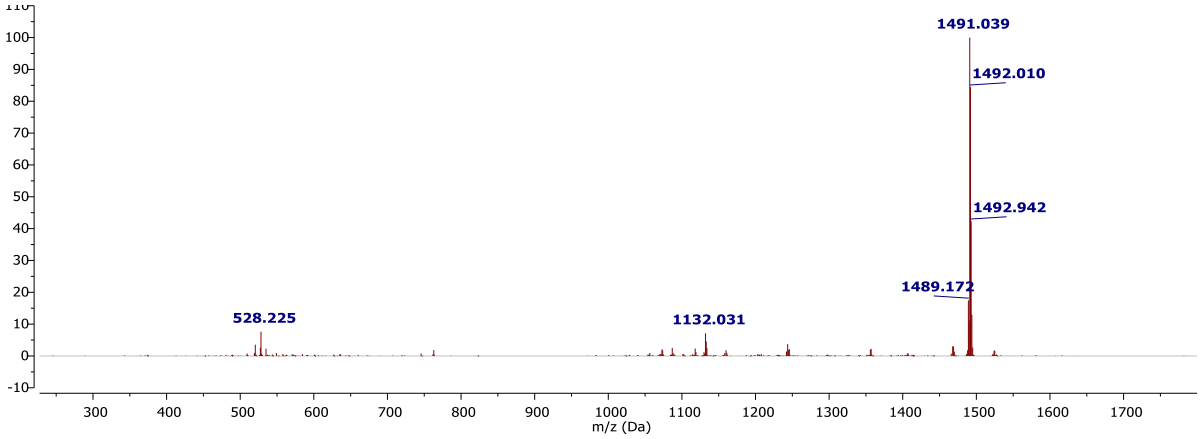

Figure S5. ESI Mass spectrum of $[LFe_3(PhPz)_3ONa][OTf]$ recorded in Acetonitrile.

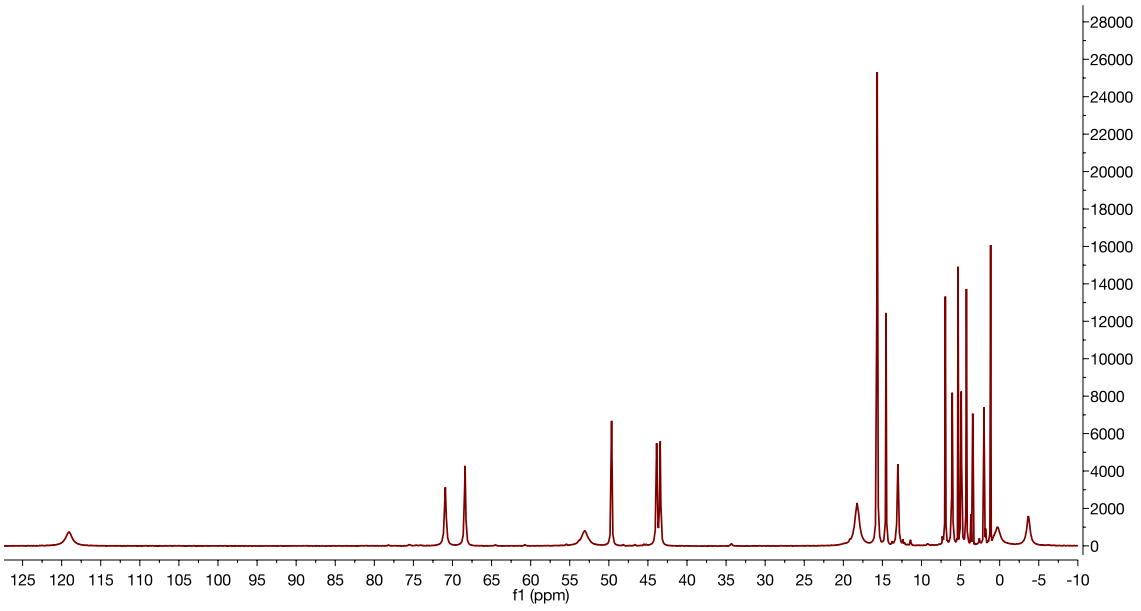

Figure S6. ^{1}H-NMR spectrum (300 MHz) of $[LFe_3(PhPz)_3OFe][OTf]_2$ in CD_2Cl_2.

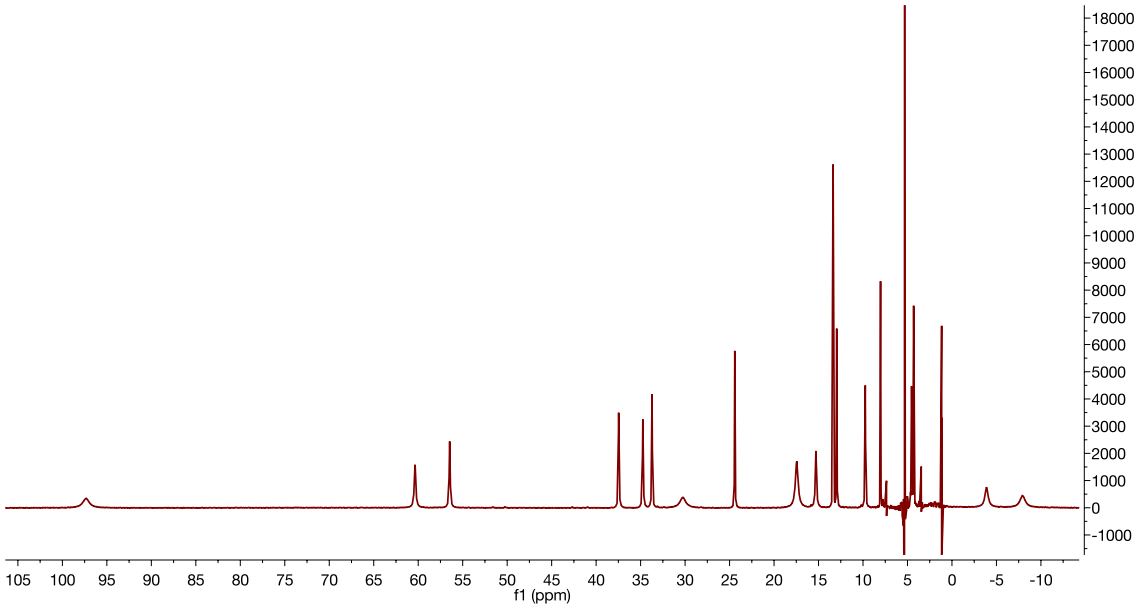

Figure S7. ^{1}H NMR spectrum (300 MHz) of $[LFe_3(PhPz)_3OFe][OTf]$ in CD_2Cl_2.

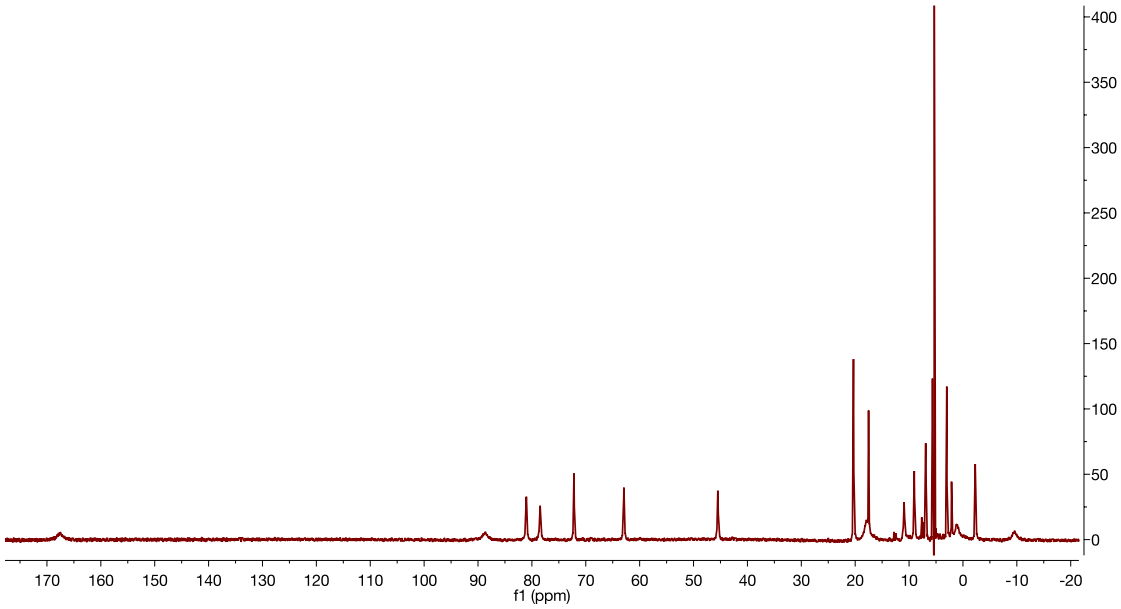

Figure S8. ^{1}H NMR spectrum (300 MHz) of $[LFe_3(PhPz)_3OFe][OTf]_3$ in CD_2Cl_2.

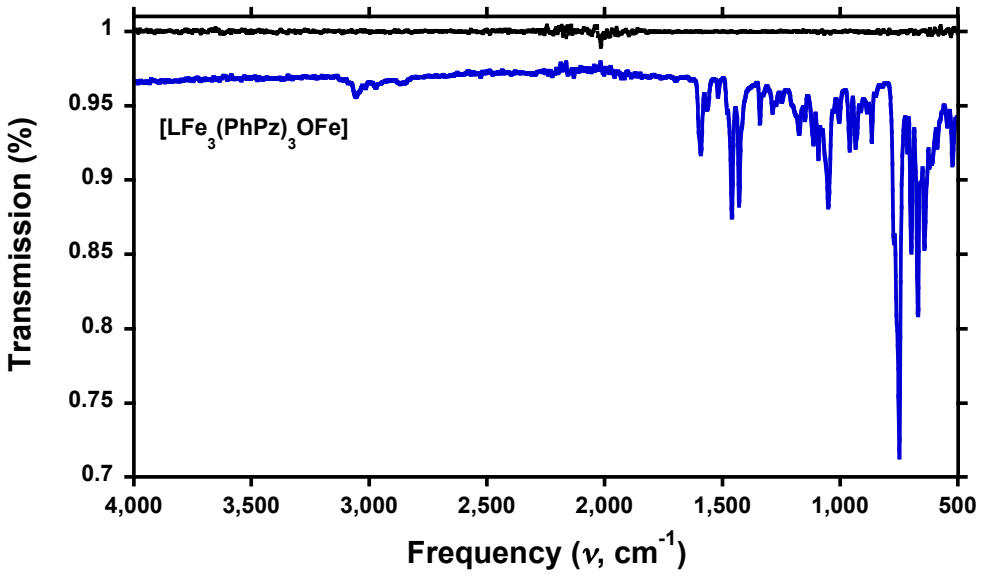

Figure S9. Solid state IR spectrum of $[LFe_3(PhPz)_3OFe]$. The black trace is the background

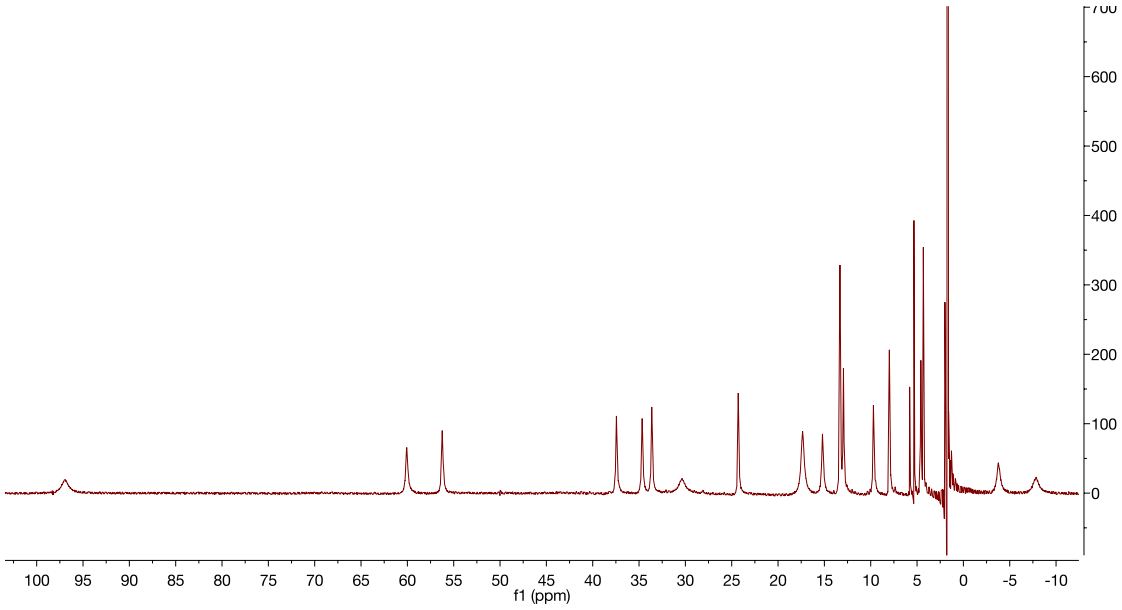

Figure S10. ^{1}H-NMR spectrum (300 MHz) of $[LFe_3(PhPz)_3OFe][OTf]$ in CD_2Cl_2. The ^{1}H NMR spectrum was obtained from the crude reaction mixture upon of $[LFe_3(PhPz)_3OFe]$ and 1.0 equiv. AgOTf. (See Page 2 for the experimental procedure).

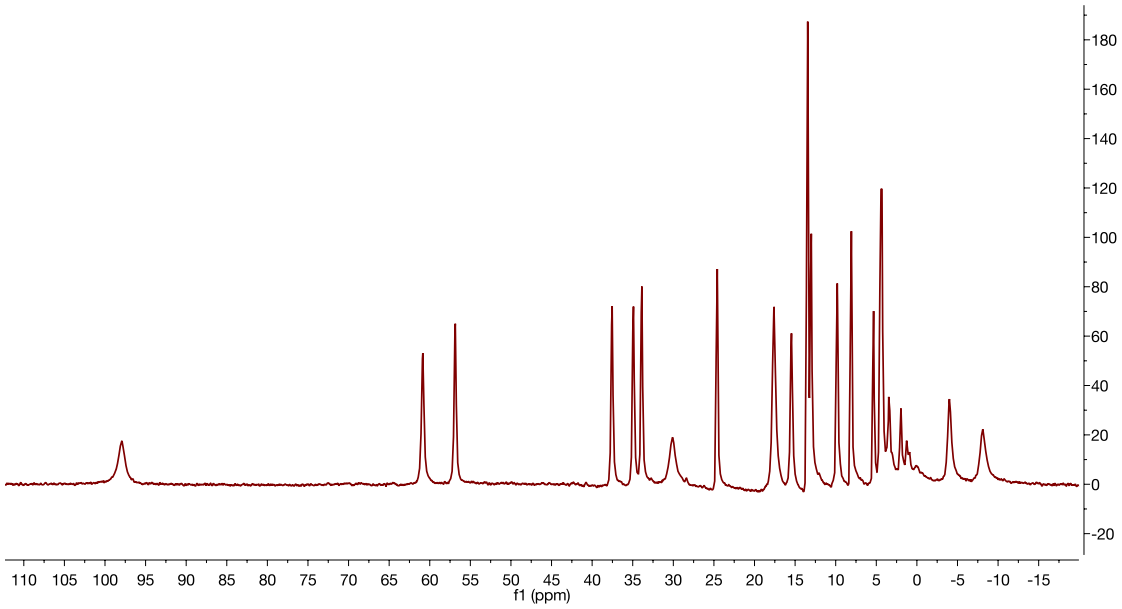

Figure S11. ^{1}H NMR spectrum (300 MHz) of $[LFe_3(PhPz)_3OFe][BF_4]$ in CD_2Cl_2. The ^{1}H NMR spectrum was obtained from the crude reaction mixture upon reaction of $[LFe_3(PhPz)_3OFe]$ with 1.0 equiv. $AgBF_4$. (See Page 2 for the experimental procedure).

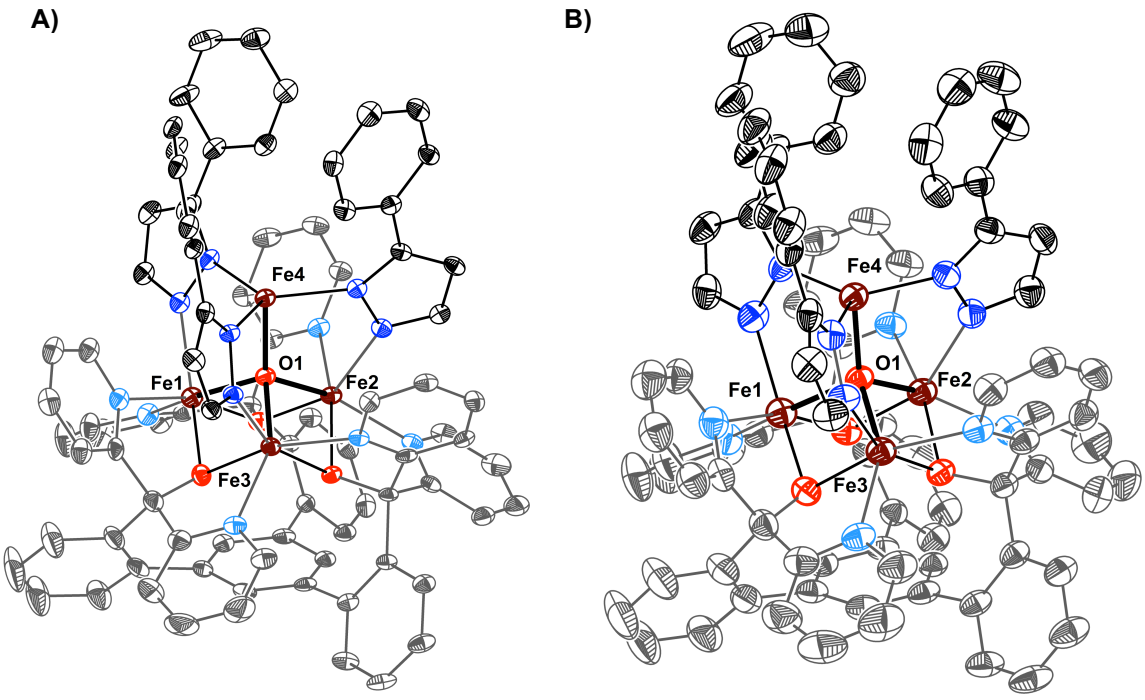

Figure S12. Crystal structure of $[LFe_3(PhPz)_3OFe][BF_4]$ at 100 K (A) and at 298 K (B). Ellipsoids are shown at the 50% probability level. Hydrogen atoms, co-crystallized solvent molecules and outer sphere counter ions are not shown for clarity.

Special Refinement Details for $[LFe_3(PhPz)_3OFe][BF_4]$ at 100K (3a). The structure contains two co-crystallized diethyl ether molecules. The first molecule is disordered over three positions that refined with occupancies of 34.8% (O200 through C203); 34.8% (O400 through C403); 30.5% (C300 through C303), with the partial disordered diethyl ether molecules (O200 through C203 and O400 through C403) close to a special position. The 1,2 and 1,3 distances in the diethyl ether molecules were refined with similarity restraints and set to be equivalent with respect to the second diethyl ether molecule (O100 through C103). The distances in the second diethyl ether molecule (O100 through C103) were restrained at 1.517 Å (C100–C101 and C102–C103), 1.411 Å (C101–O100 and C102–O100), 2.309 Å (C101–C102), and 4.743 Å (C100–C103). Enhanced rigid bond restraints were used on all disordered diethyl ether molecules while additional isotropic restraints were used on all disordered diethyl ether molecules (O100 through C103 and O400 through C403. Atoms O200 through C203, and O400 through C403, C101 and C100, were set to have equivalent anisotropic displacement parameters.

Special Refinement Details for $[LFe_3(PhPz)_3OFe][BF_4]$ at 298K (3b). The structure contains two co-crystallized diethyl ether molecules. The first molecule is disordered over three positions that refined with occupancies of 34.8% (O200 through C203); 34.8% (O400 through C403); 30.5% (C300 through C303), with the partial disordered diethyl ether molecules (O200 through C203 and O400 through C403) close to a special position. The 1,2 and 1,3 distances in the diethyl ether molecules were refined with similarity restraints and set to be equivalent with respect to the second diethyl ether molecule (O100 through C103). The distances in the second diethyl ether molecule (O100 through C103) were restrained at 1.517 Å (C100–C101 and C102–C103), 1.411 Å (C101–O100 and C102–O100), 2.309 Å (C101–C102), and 4.743 Å (C100–C103). Enhanced rigid bond restraints were used on all disordered diethyl ether molecules while additional isotropic restraints were used on some disordered diethyl ether molecules (O100 through C103 and O400 through C403. Atoms C200 and C201, C401 and C400, C101 and C100, were set to have equivalent anisotropic displacement parameters.

Table S1. Crystal and refinement data for complexes **3a** and **3b**.

	Complex **3a**	Complex **3b**
Empirical formula	$C_{92}H_{80}BF_4Fe_4N_{12}O_6$	$C_{92}H_{80}BF_4Fe_4N_{12}O_6$
Formula weight (g/mol)	1759.89	1759.89
T (K)	100.0	298.0
Radiation	MoKα (λ = 0.71073)	MoKα (λ = 0.71073)
a (Å)	40.239(2)	40.491(4)
b (Å)	17.7901(11)	18.033(2)
c (Å)	25.3164(14)	25.553(2)
α (deg)	90	90
β (deg)	113.3992(17)	113.323(3)
γ (deg)	90	90
V (Å^3)	16632.6(17)	17133(3)
Z	8	8
Cryst. syst.	monoclinic	monoclinic
Space group	C2/c	C2/c
ρ_{calc}g (cm^3)	1.406	1.365
2 σ range (deg)	4.39 to 60.2	4.35 to 61.078
Crystal size/mm	0.21 × 0.04 × 0.01	0.21 × 0.04 × 0.01
μ (mm^{-1})	0.756	0.734
GOF	1.036	1.016
R1, wR (I> 2σ (I))	0.0924, 0.2092	0.0760, 0.1468

Table S2. Selected bond distances for complexes **3a** and **3b.**

Bond Distance (Å)	**Complex**	
	3a	**3b**
Fe1–O1	2.082(3)	2.048(2)
Fe2–O1	2.102(3)	2.068(2)
Fe3–O1	1.889(3)	1.954(2)
Fe4–O1	1.901(3)	1.902(2)
Fe1–N13	2.153(4)	2.151(3)
Fe2–N23	2.166(4)	2.173(3)
Fe3–N33	2.130(4)	2.138(3)
Fe4–N14	2.067(4)	2.077(3)
Fe4–N24	2.073(4)	2.077(3)
Fe4–N34	2.112(4)	2.101(3)
N13–N14	1.387(6)	1.383(4)
N23–N24	1.391(5)	1.380(4)
N33–N34	1.385(6)	1.384(4)

Table S3. Variable temperature Mössbauer parameters for complex $[LFe_3(PhPz)_3OFe][BF_4]$ recorded at 80K, 100k, 200K and 298 K.

#	Temperature (K)	$[LFe_3(PhPz)_3OFe][BF_4]$	
		δ (mm/s)	$\lvert \Delta E_q \rvert$ (mm/s)
1	80 K	0.509	1.036
		1.117	3.172
		1.134	3.484
		0.916	2.375
2	100 K	0.524	1.045
		1.090	3.017
		1.119	3.369
		0.846	2.092
3	200 K	0.437	1.405
		1.031	2.246
		1.042	3.080
		0.879	1.126
4	298 K	0.281	1.378
		0.756	2.143
		1.079	2.545
		0.842	0.809

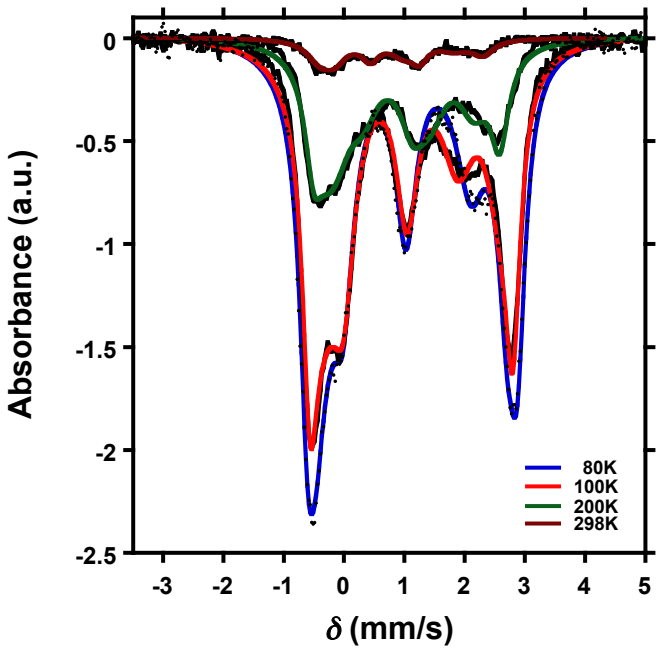

Figure S13. Variable temperature (VT) zero-field ^{57}Fe Mossbauer spectrum of $[LFe_3(PhPz)_3OFe][BF_4]$ recorded at 80K (not shown), 100k (blue trace), 200K (red trace) and 298K (green trace).

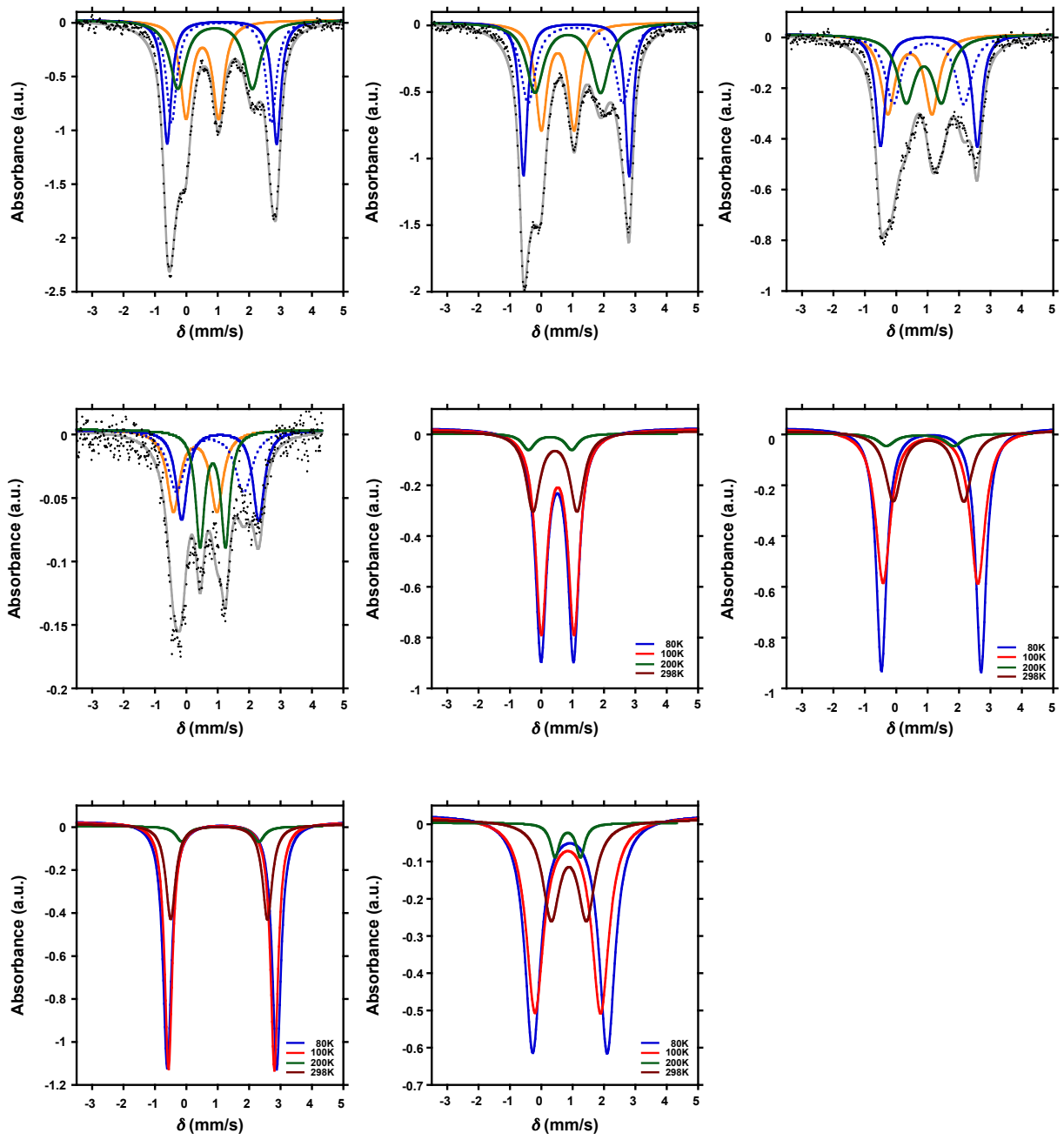

Figure S14. Variable temperature (VT) zero-field ^{57}Fe Mössbauer spectra (including fits) of $[LFe_3(PhPz)_3OFe][BF_4]$ recorded at 80K (A) 100 K (B), 200 K (C) and 298 K (D). Figures E-H show the individual fits recorded at 80 K (blue trace), 100 K (red trace), 200 K (brown trace), and 298 K (green trace) for the Fe^{III} metal centers (E), Fe^{II} metal centers (F and G), and the apical Fe^{II} metal center (H). The plots demonstrate the consistency of the isomer shift (*d*) and the narrowing of the quadrupole splitting ($|\Delta E_q|$) upon on temperature variation (Table S3).

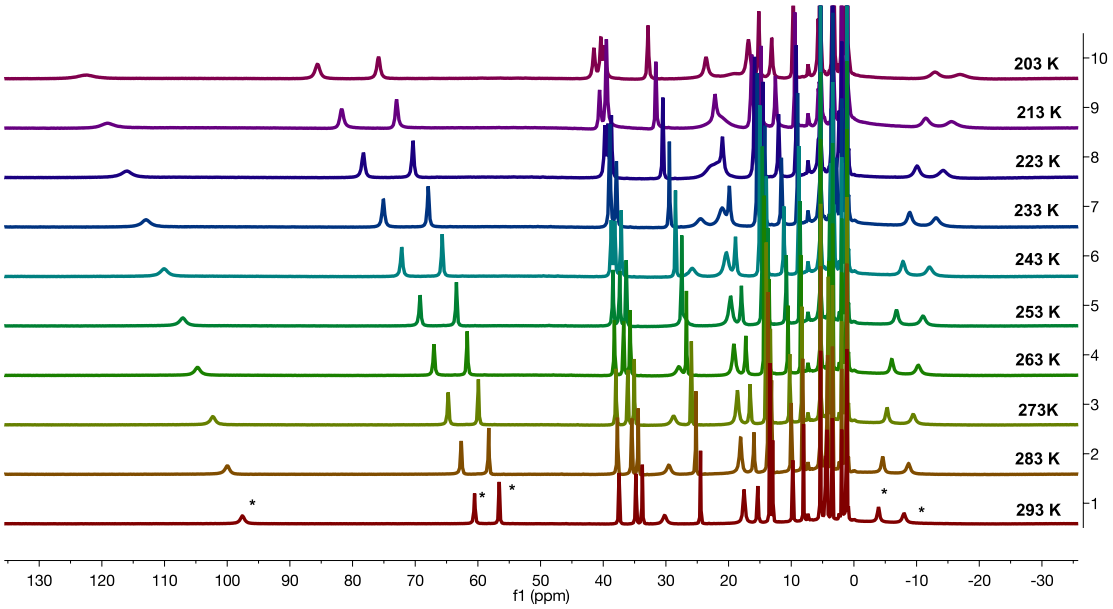

Figure S15. Variable temperature (VT) ^{1}H NMR spectrum (400 MHz) of $[LFe_3(PhPz)_3OFe][BF_4]$ in CD_2Cl_2 recorded between 203 and 293 K.

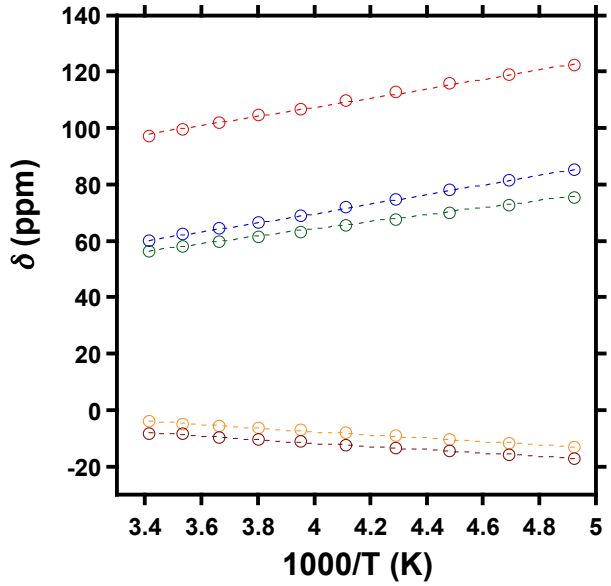

Figure S16. Curie plot showing the linear dependence (vs. the inverse temperature) of the ^{1}H chemical shift of selected protons (highlighted in Figure S15) in $[LFe_3(PhPz)_3OFe][BF_4]$ between 203 and 293 K. The dashed lines are a guide to the eye.

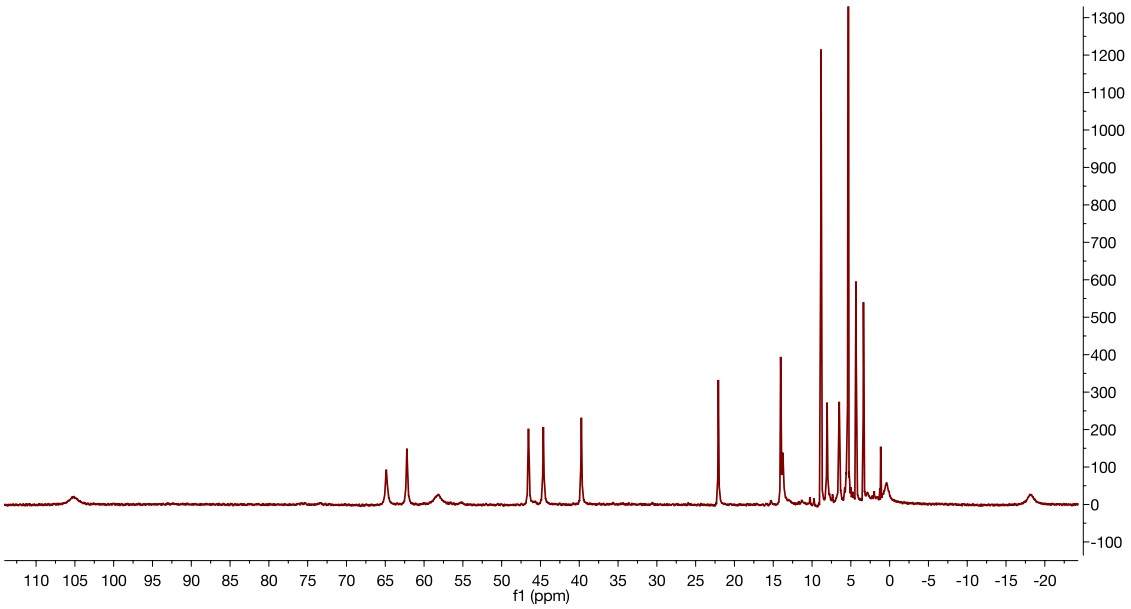

Figure S17. ^{1}H NMR spectrum (300 MHz) of $[LFe_3(PhPz)_3OFe(NO)][OTf]$ in CD_2Cl_2.

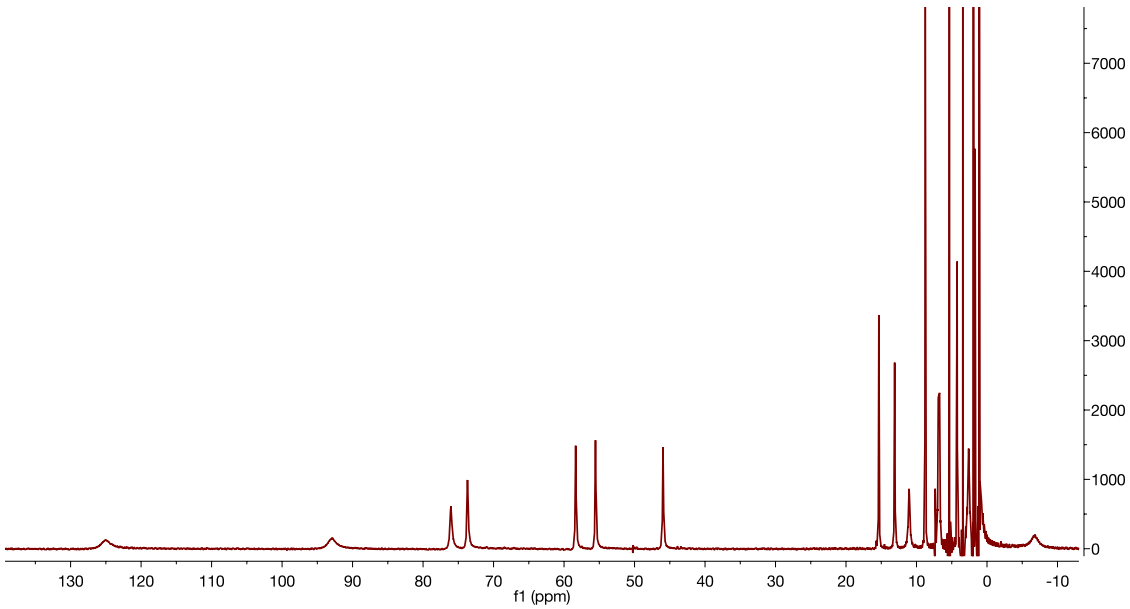

Figure S18. ^{1}H NMR spectrum (300 MHz) of $[LFe_3(PhPz)_3OFe(NO)][OTf]_2$ in CD_2Cl_2.

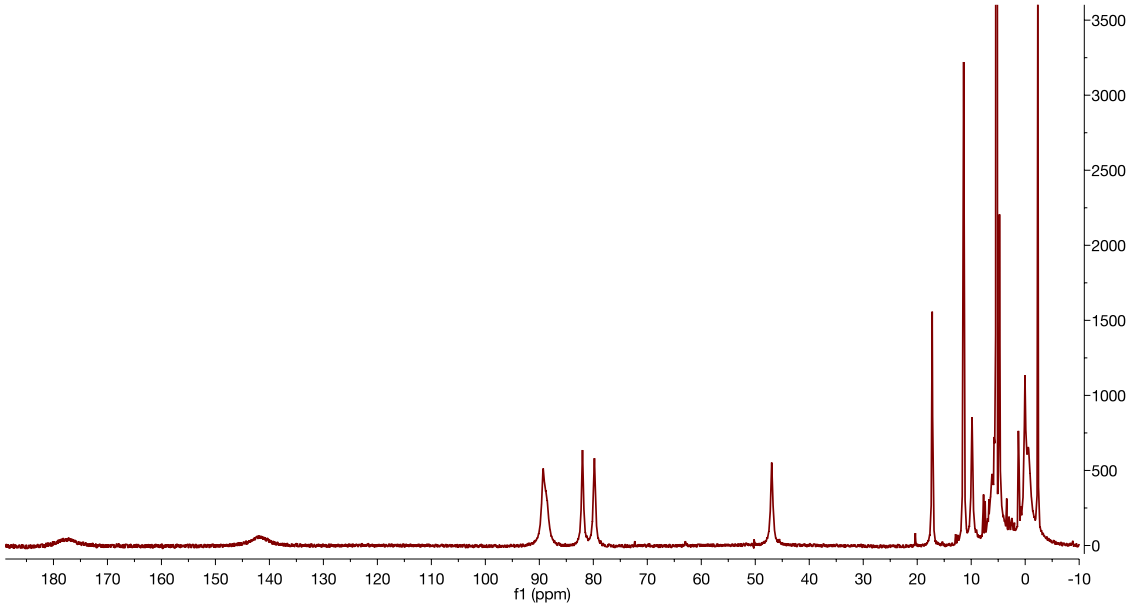

Figure S19. ^{1}H NMR spectrum (300 MHz) of [LFe^{3}(PhPz)$_3$OFe(NO)][OTf]$_3$ in CD_2Cl_2.

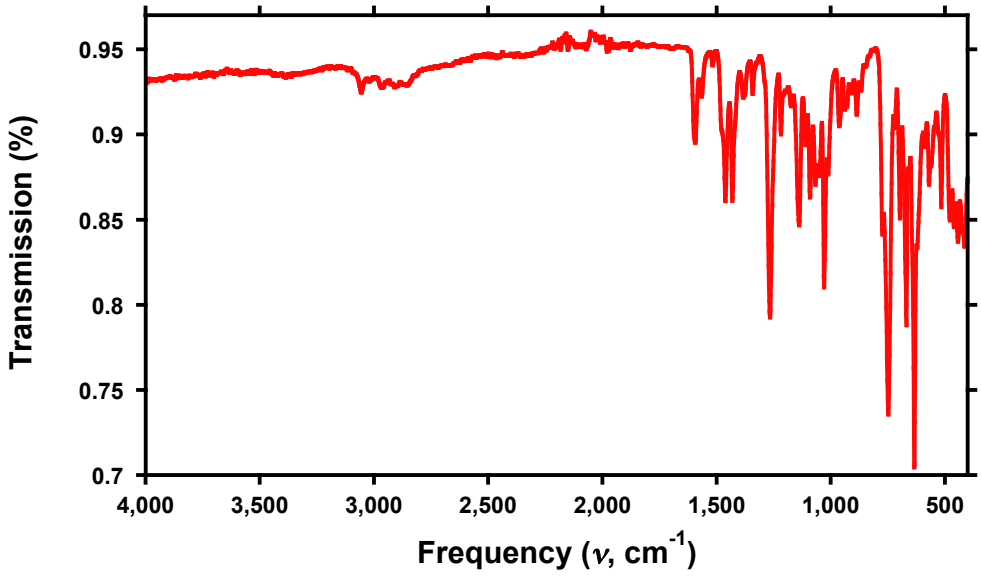

Figure S20. Solid state IR spectrum of the crude reaction mixture upon reaction of $CoCp^{*}_2$ (1.25 equiv.) and [LFe$_3$(PhPz)$_3$OFe(NO)][OTf] (1.0 equiv). The black trace is the background

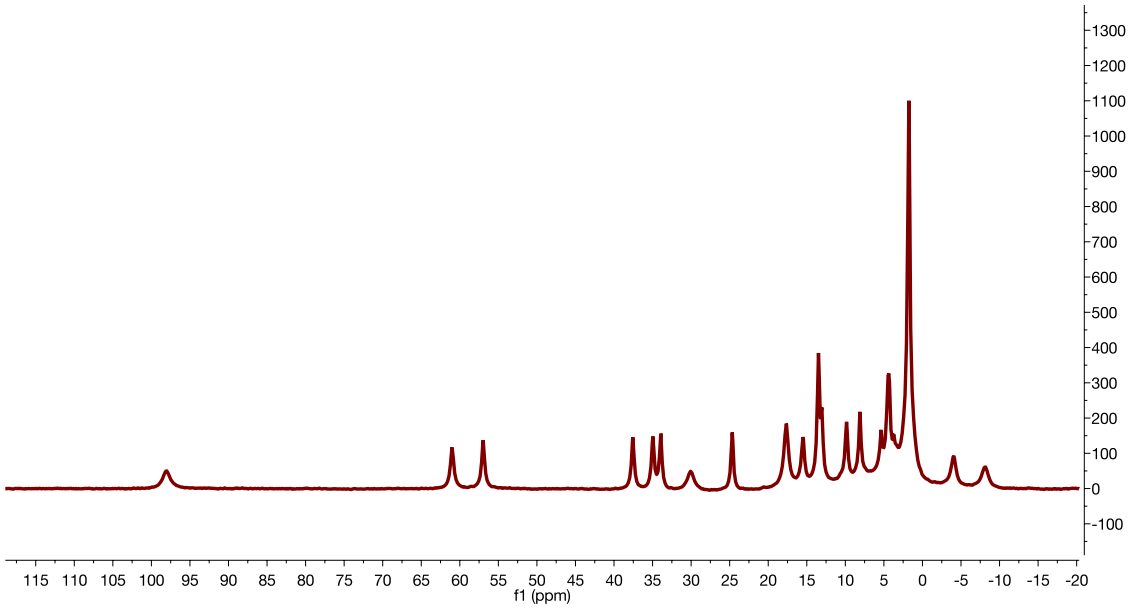

Figure S21. ^{1}H NMR spectrum (300 MHz) of the crude reaction mixture upon reaction of $CoCp^{*}_{2}$ (1.25 equiv. and $[LFe_3(PhPz)_3OFe(NO)][OTf]$ (1.0 equiv.).

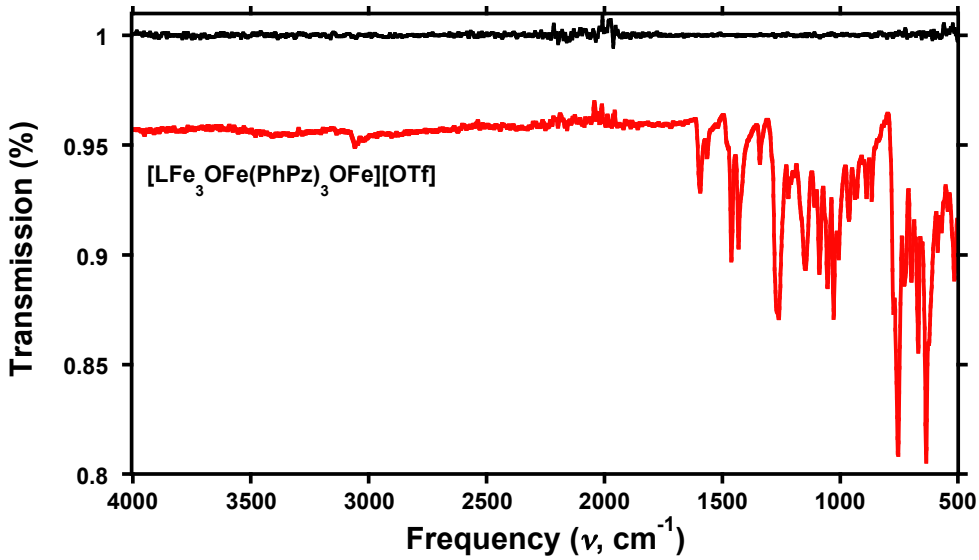

Figure S22. Solid state IR spectrum of $[LFe_3(PhPz)_3OFe][OTf]$. The black trace is the background

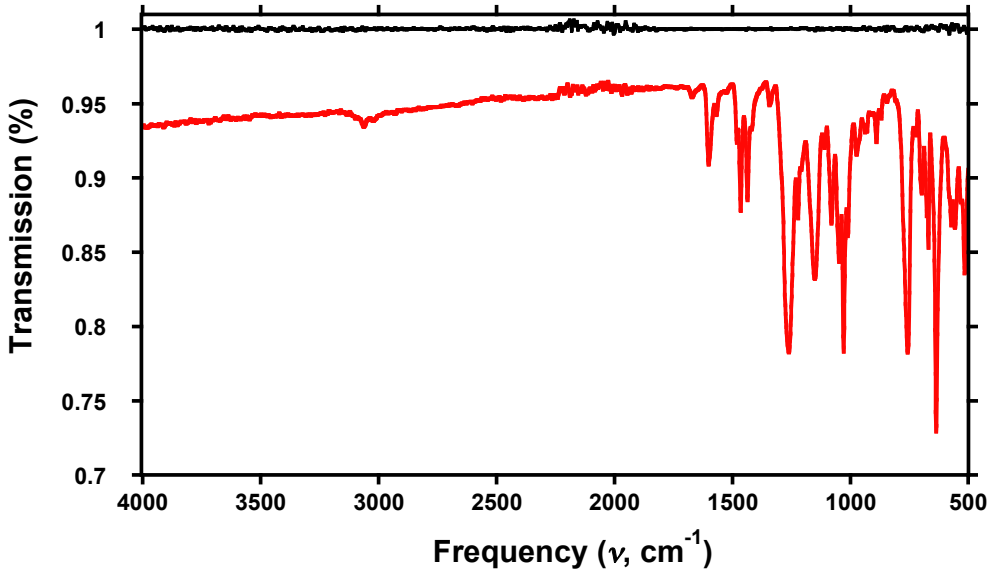

Figure S23. Solid state IR spectrum of $[LFe_3(PhPz)_3OFe][OTf]_2$. The black trace is the background

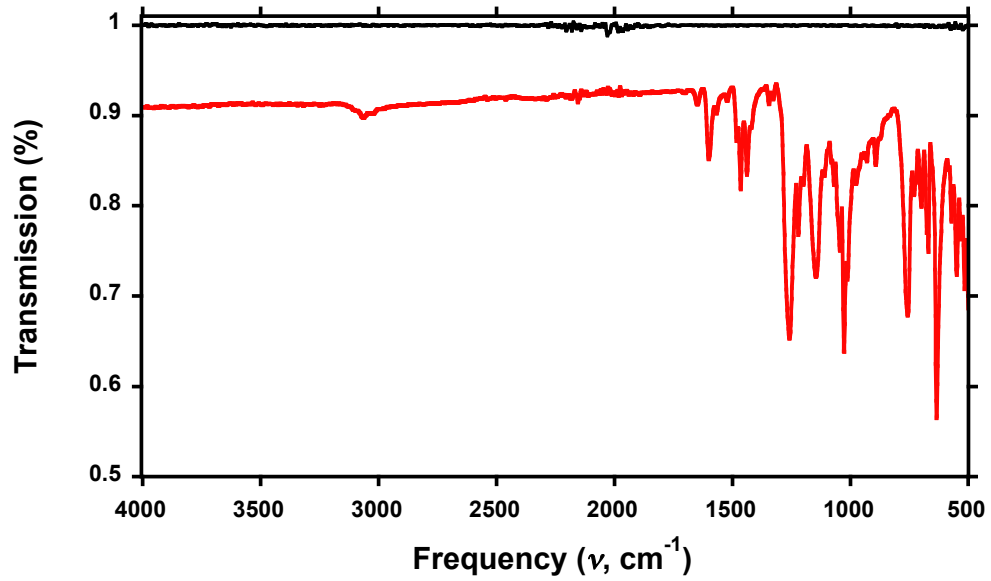

Figure S24. Solid state IR spectrum of $[LFe_3(PhPz)_3OFe][OTf]_3$. The black trace is the background

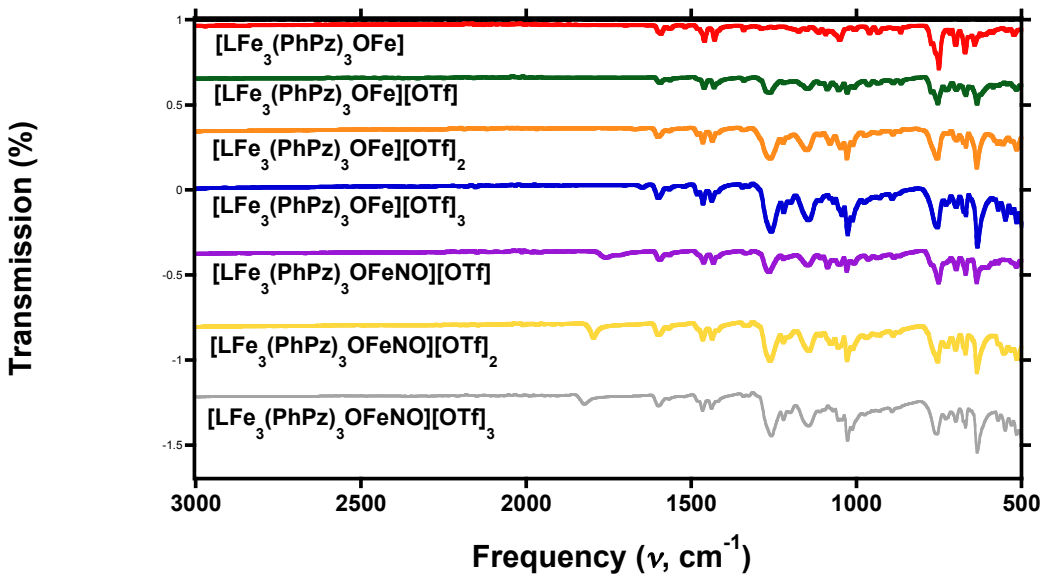

Figure S25. Overview of the solid-state IR spectra of complexes **2**-**8**.

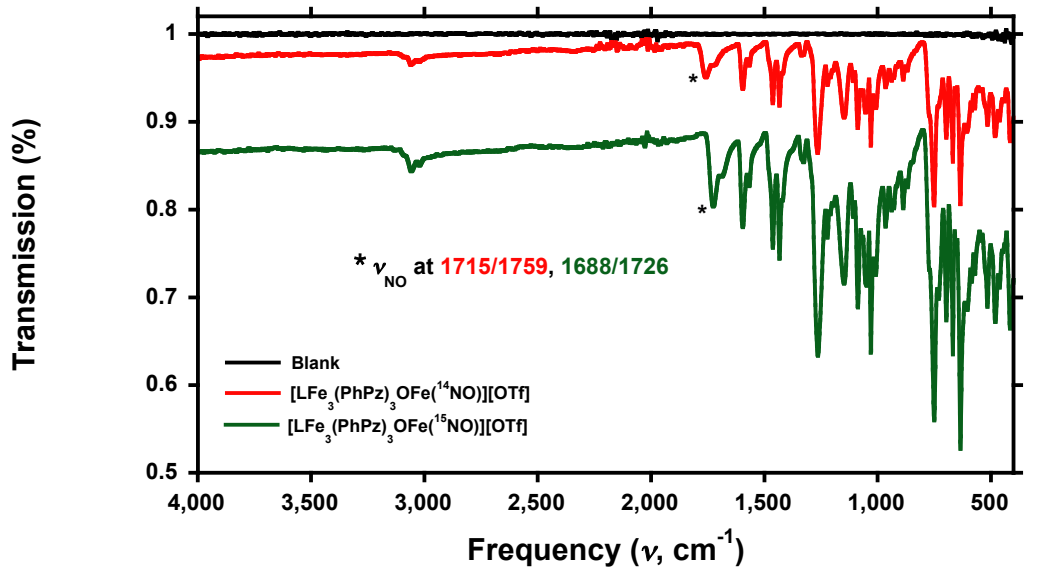

Figure S26. IR spectra of $[LFe_3(PhPz)_3OFe(^{14}NO)][OTf]$ and $[LFe_3(PhPz)_3OFe(^{15}NO)][OTf]$.

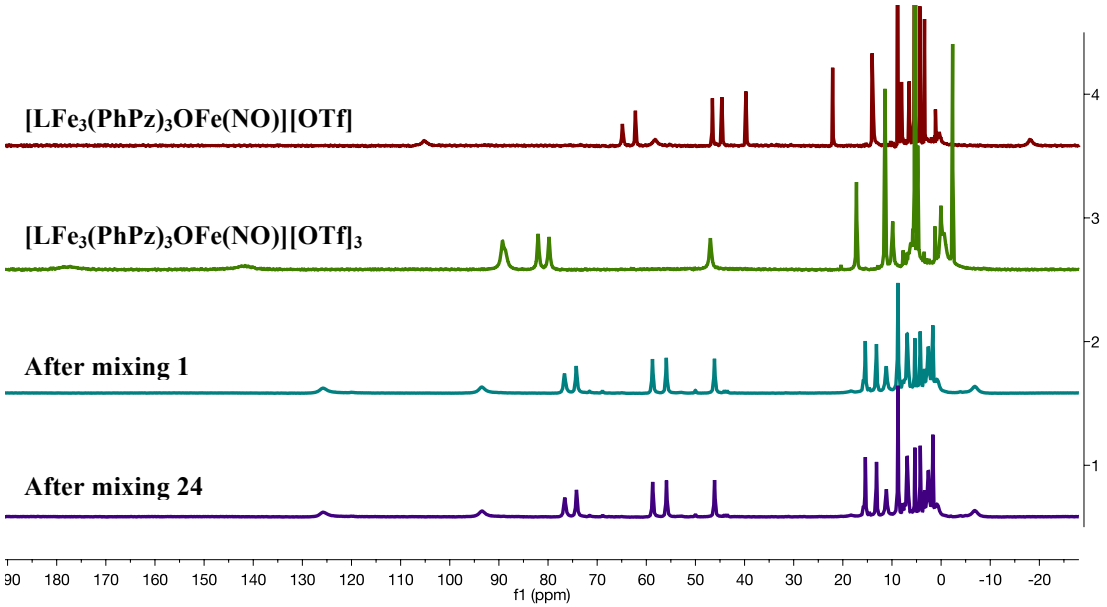

Figure S27. ^{1}H NMR spectrum (300 MHz) of the crude reaction mixture upon mixing $[LFe_3(PhPz)_3OFe(NO)][OTf]$ (red trace) and $[LFe_3(PhPz)_3OFe(NO)][OTf]_3$ (green trace) taken after 1 hour (magenta trace) and 24 hours (purple trace). The magenta and purple trace are identical to that of $[LFe_3(PhPz)_3OFe(NO)][OTf]_2$ (Figure S18).

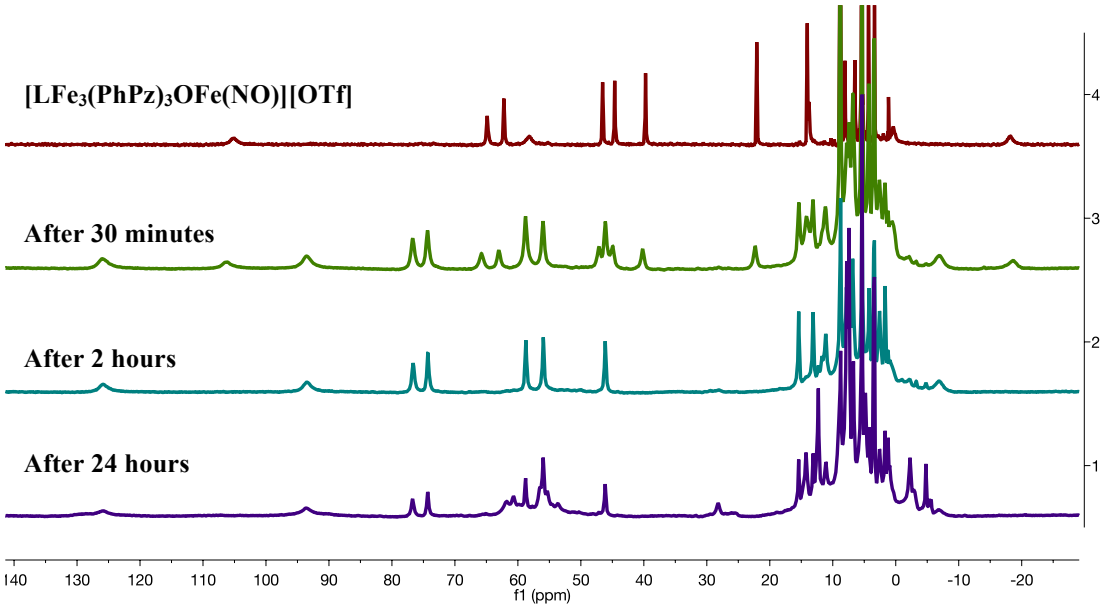

Figure S28. ^{1}H NMR spectrum (300 MHz) of the crude reaction mixture upon addition of 1 atm. O_2 to solution of $[LFe_3(PhPz)_3OFe(NO)][OTf]$ (red trace) in a J-Young NMR tube. The ^{1}H NMR spectra were recorded after 0.5 hour (green trace), 2 hours (magenta trace), and 24 hours (purple trace). Note that the spectra recorded after 2 hours (magenta trace) is identical to that of $[LFe_3(PhPz)_3OFe(NO)][OTf]_2$ (Figure S18).

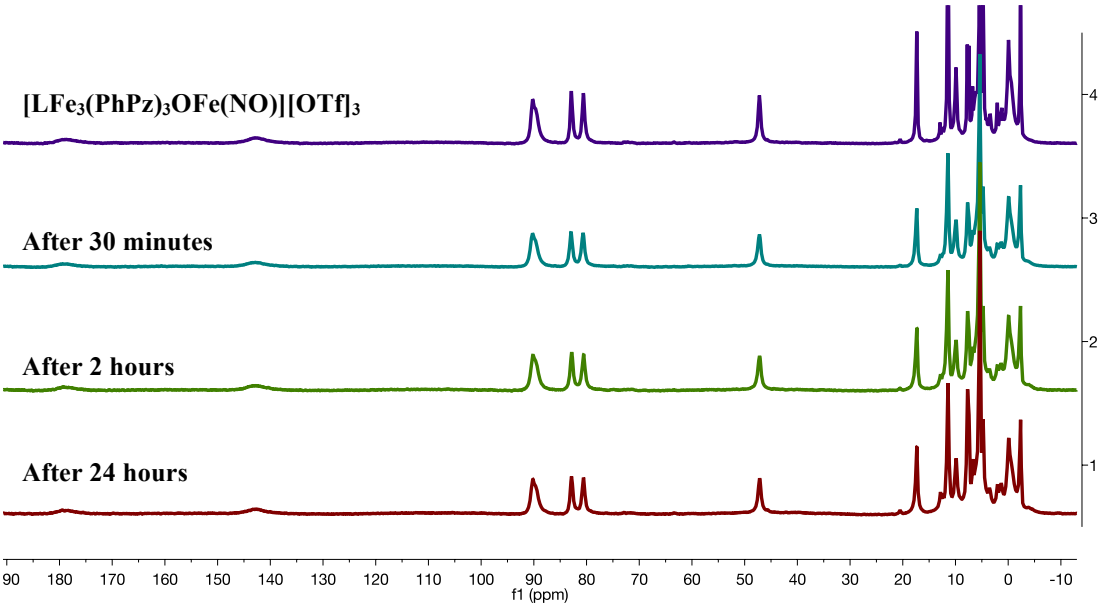

Figure S29. ^{1}H NMR spectrum (300 MHz) of the crude reaction mixture upon addition of 1 atm. O_2 to solution of $[LFe_3(PhPz)_3OFe(NO)][OTf]_3$ (red trace) in a J-Young NMR tube. The ^{1}H NMR spectra were recorded after 0.5 hour (green trace), 2 hours (magenta trace), and 24 hours (purple trace).

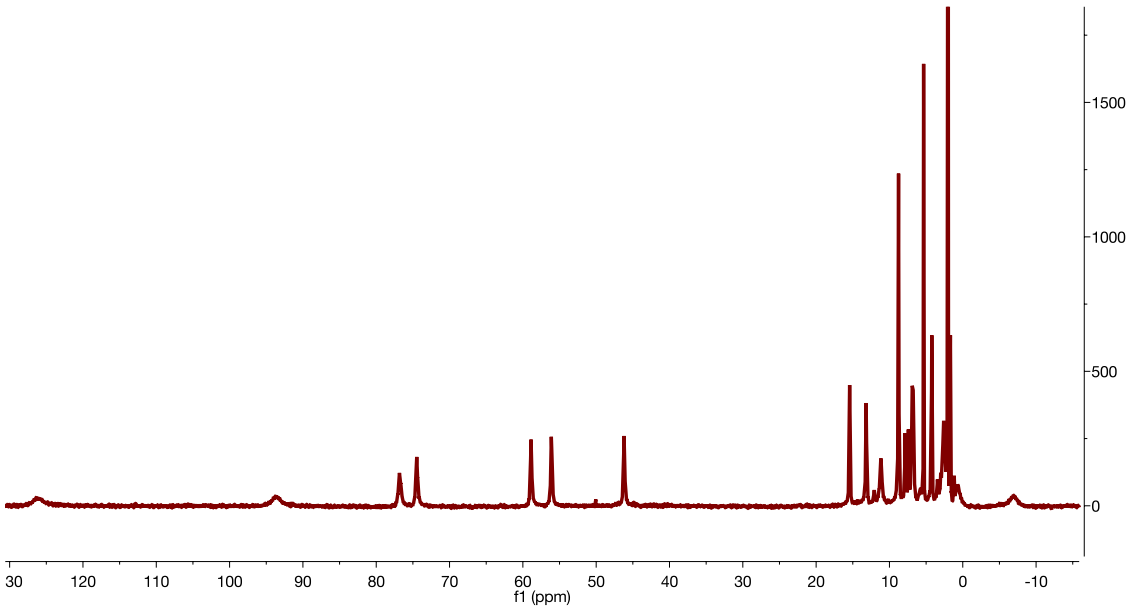

Figure S30. ^{1}H NMR spectrum (300 MHz) of the crude reaction mixture upon addition of 6 equiv. to $[LFe_3(PhPz)_3OFe(NO)][OTf]_1$ recorded after 28 h, after vacuum transfer of all volatiles. The ^{1}H NMR spectrum is identical to that of $[LFe_3(PhPz)_3OFe(NO)][OTf]_2$ (Figure S18).

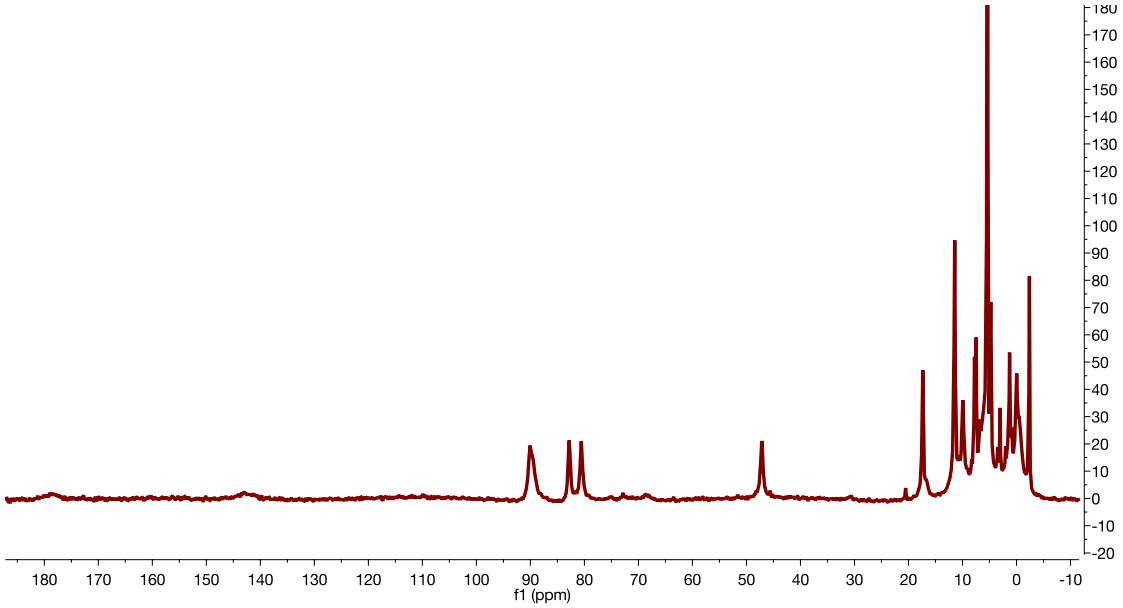

Figure S31. ^{1}H NMR spectrum (300 MHz) of the crude reaction mixture upon addition of 6 equiv. to $[LFe_3(PhPz)_3OFe(NO)][OTf]_3$ recorded after 28 h, after vacuum transfer of all volatiles. The ^{1}H NMR spectrum is identical to that of $[LFe_3(PhPz)_3OFe(NO)][OTf]_3$ (Figure S19).

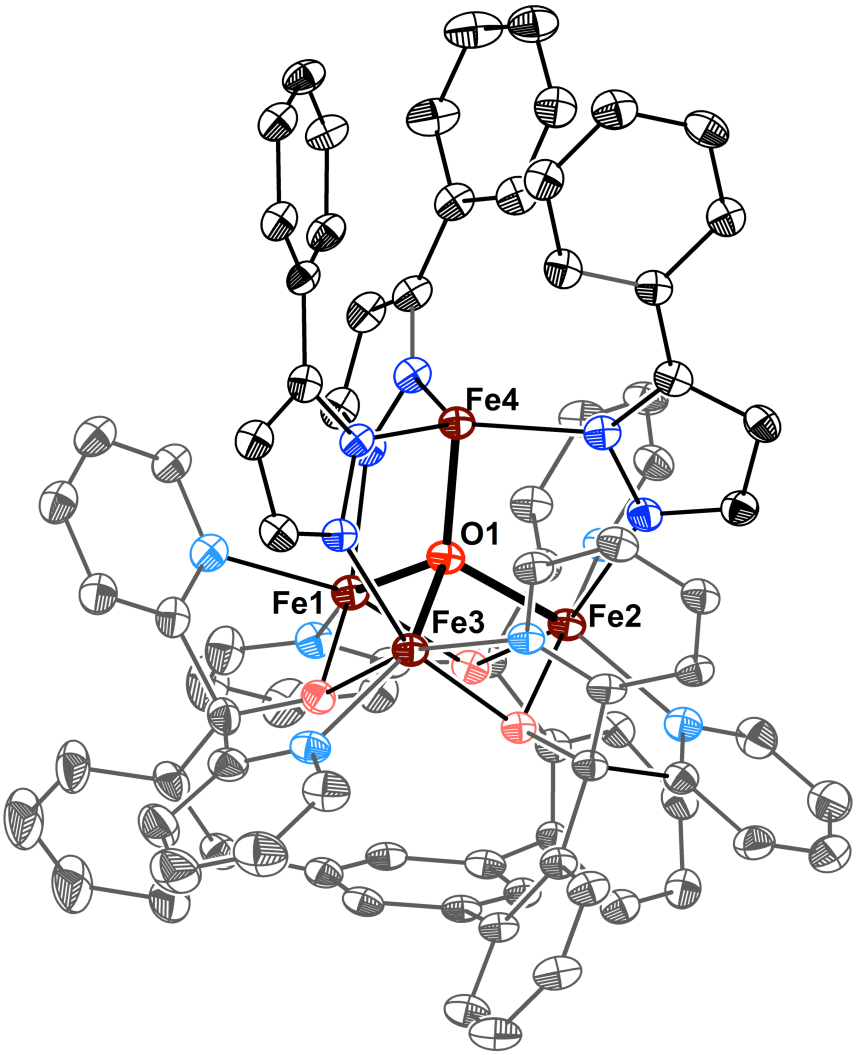

Figure S32. Crystal structure of $[LFe_3(PhPz)_3OFe][BF_4]$. Ellipsoids are shown at the 50% probability level. Hydrogen atoms, co-crystallized solvents and outer sphere counter ions are not shown for clarity.

Special Refinement Details for $[LFe_3(PhPz)_3OFe][BF_4]$ (3). The structure contains two co-crystallized diethyl ether molecules. The first molecule is disordered over three positions that refined with occupancies of 34.8% (O200 through C203); 34.8% (O400 through C403); 30.5% (C300 through C303), with the partial disordered diethyl ether molecules (O200 through C203 and O400 through C403) close to a special position. The 1,2 and 1,3 distances in the diethyl ether molecules were refined with similarity restraints and set to be equivalent with respect to the second diethyl ether molecule (O100 through C103). The distances in the second diethyl ether molecule (O100 through C103) were restrained at 1.517 Å (C100–C101 and C102–C103), 1.411 Å (C101–O100 and C102–O100), 2.309 Å (C101–C102), and 4.743 Å (C100–C103). Enhanced rigid bond restraints were used on all disordered diethyl ether molecules while additional isotropic restraints were used on some disordered diethyl ether molecules (O100 through C103 and O400 through C403. Atoms C200 and C201, C401 and C400, C101 and C100, were set to have equivalent anisotropic displacement parameters.

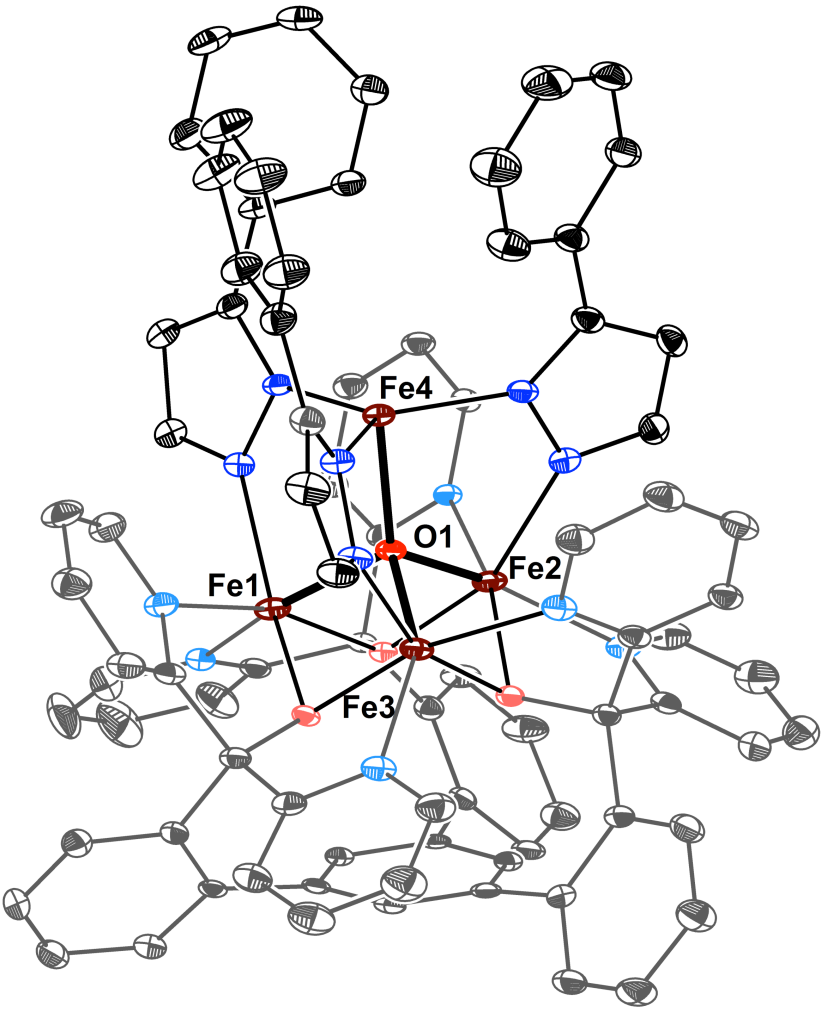

Figure S33. Crystal structure of $[LFe_3(PhPz)_3OFe][OTf]_2$. Ellipsoids are shown at the 50% probability level. Hydrogen atoms, co-crystallized solvents and outer sphere counter ions are not shown for clarity.

Special Refinement Details for $[LFe_3(PhPz)_3OFe][OTf]_2$ (4). The structure contains two triflate counter ions, from which one is disordered over two positions that refined with occupancies of 57.8% (S401 through C401) and 42.2% (S402 through C402). The 1,2 and 1,3 distances in the disordered triflate were refined with similarity restraints and set to be equivalent with respect to the first triflate counter ion (S400 through C400). Enhanced rigid bond restraints were used on the disordered triflate counter ions. Furthermore, the structure contains several disordered co-crystallized solvent molecules. The bond distances of a single diethyl ether (O200 through C211) were restrained at 1.517 Å (C208–C209 and C210–C211), 1.411 Å (C209–O200 and C110–O200), 2.376 Å (C208–O200 and C211–O200), while the bond distances of a single co-crystallized acetonitrile (C304 through N302) were restrained at 1.458 Å (C304–C305) and at 1.157 (C304–N302). These two solvent molecules were used to refine the 1,2 and 1,3 distances bond distances with similarity restraints on all the remaining co-crystallized acetonitrile and diethyl ether solvents (C300 through N300); (C302 through N301; (C306 through N303); (O201 through C203); and (O202 through C207) molecules. Enhanced rigid bond restrains were used on disordered solvents (C306 through N303) and (O202 through C207). Atoms C204 and C205, C202, C201 were set to have equivalent anisotropic displacement parameters. Furthermore, the co-crystallized diethyl ether solvents (O201 through C203); and (O202 through C207) and the acetonitrile solvent (C306 through N303) molecule are disordered over a similar position with partial occupancies of 36.5 % (O202 through C207), 36.5 % (C306 through N303), and 27.0 % (O201 through C203), while being close to a special position. In addition the co-crystallized diethyl ether (O200 through C211), and the acetonitrile (C302 through N301) solvents are close to special positions as well.

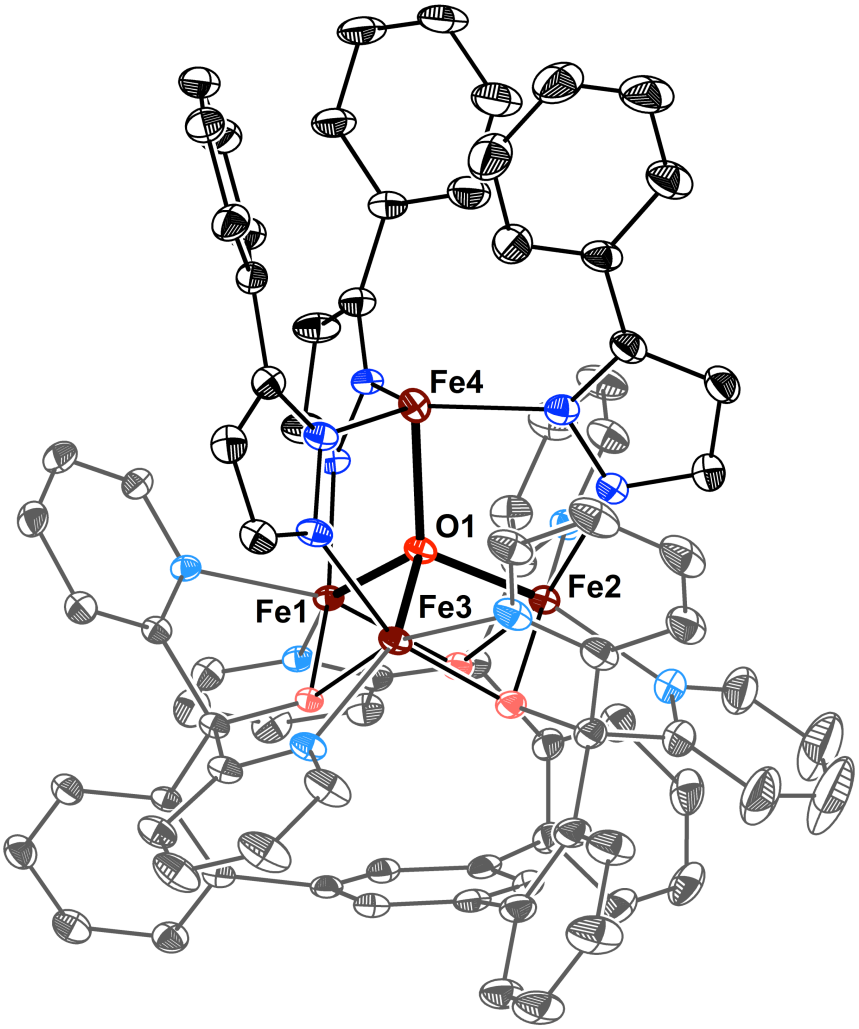

Figure S34. Crystal structure of $[LFe_3(PhPz)_3OFe][OTf]_3$. Ellipsoids are shown at the 50% probability level. Hydrogen atoms, co-crystallized solvents and outer sphere counter ions are not shown for clarity.

Special Refinement Details for $[LFe_3(PhPz)_3OFe][OTf]_3$ (5). The structure contains three triflate counter ions, from which two are disordered. The first triflate counter is disordered over two positions and refined with occupancies of 31.0% (S201 through C 201) and 69.0% (S202 through C202). The second triflate counter ion is disordered over three positions that contains a disordered diethyl ether and dichloromethane molecule. The occupancies of the triflate were artificially fixed at 1 together with various contributions of the co-crystallized solvent. The final occupancies for the triflate counter ions refined as: 36.7% (S204 through C204), 26.1% (S203 through C203), and 37.2% (S205 through C205), while the various solvent contributions refined as 18.5% (O101 through C107) for the co-crystallized diethyl ether and 25.7 % (C206 through Cl2) for the dichloromethane solvent molecule. The triflate counter ion (S200 through C200) was used to refine the 1,2 and 1,3 distances with similarity restraints on all the other triflate counter ions. For the co-crystallized diethyl ether and dichloromethane molecules; diethyl ether molecule (O100 through C103) and dichloromethane molecule (C108 through Cl4) were used to refine the 1,2 and 1,3 distances with similarity restraints. For diethyl ether molecule (O100 through C103) the bond distances were restrained at 1.517 Å (C100–C101 and C102–C103), 1.411 Å (C101–O100 and C102–O100), 2.346 Å (C103–O100 and C100–O100), 2.341 Å (C103–C100), and at 4.743 Å (C103–C100). Distance restraints were used between neighboring hydrogen atoms that were in close contacts. Furthermore, the structure contains co-crystallized two dichloromethane molecules and a diethyl ether molecule disordered over a similar position that refined with occupancies of 27.1% (C109 through Cl6), 36.3% (C108 through Cl4), and 36.6% (O100 through C103). Enhanced rigid bond restraints were used on all triflates counter ions and disordered co-crystallized solvent molecules, while additional isotropic restrains were used on diethyl ether molecule (O101 through C107) and C108.

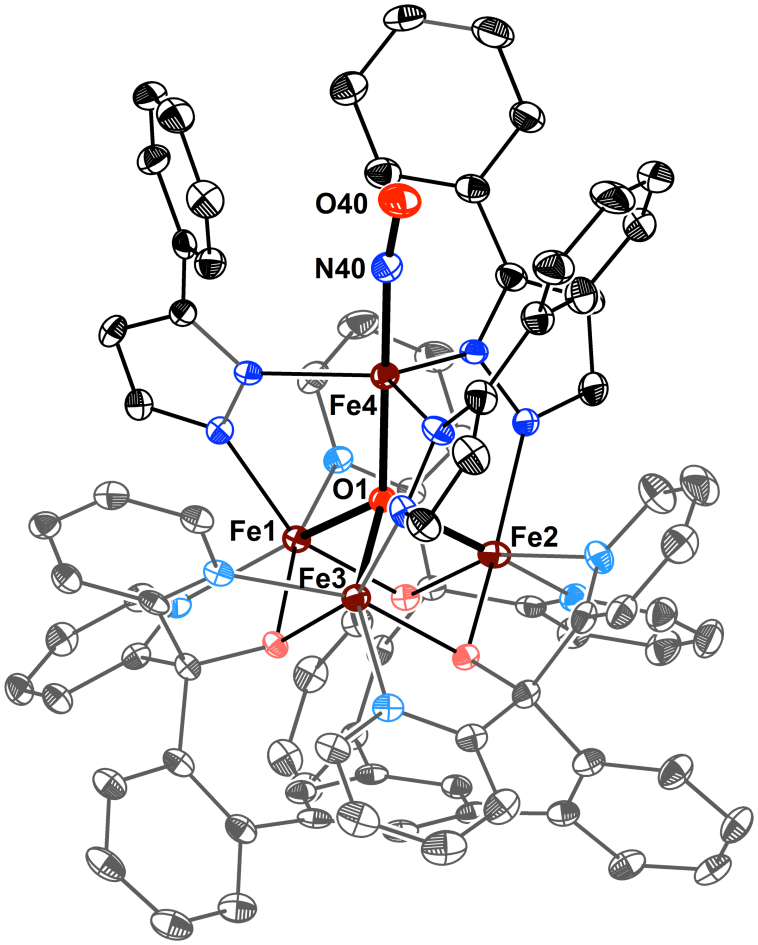

Figure S35. Crystal structure of $[LFe_3(PhPz)_3OFe(NO)][OTf]_1$. Ellipsoids are shown at the 50% probability level. Hydrogen atoms, co-crystallized solvents and outer sphere counter ions are not shown for clarity.

Special Refinement Details for $[LFe_3(PhPz)_3OFe(NO)][OTf]_1$ (6). The structure contains a single co-crystallized diethyl ether molecule (O101–C107) that is close to a special position.

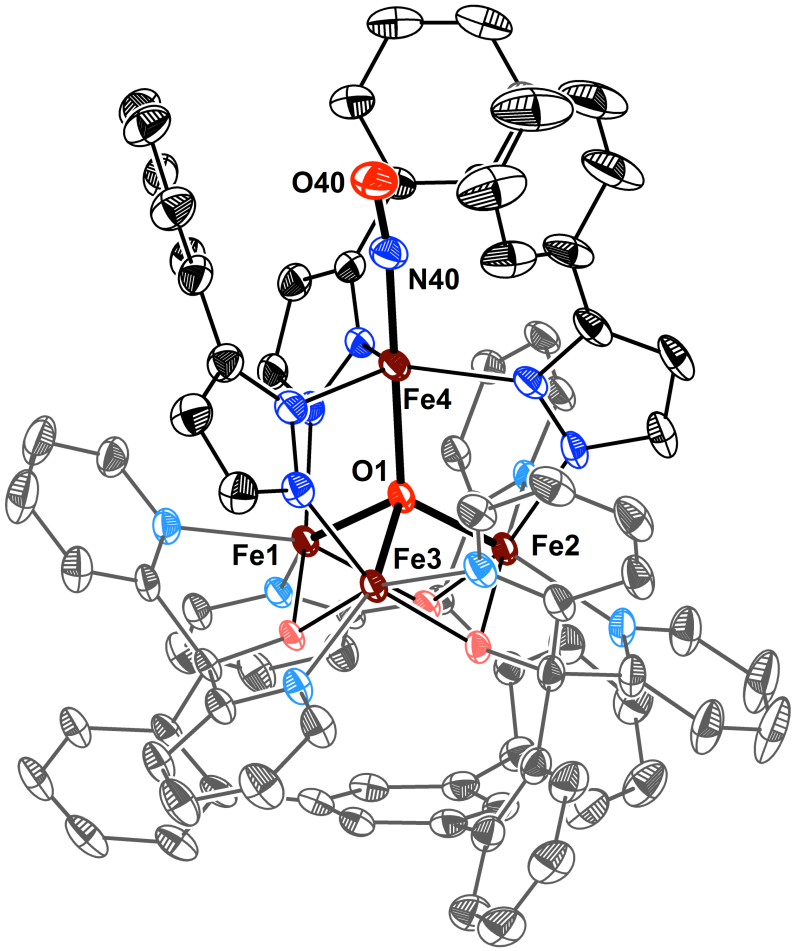

Figure S36. Crystal structure of $[LFe_3(PhPz)_3OFe(NO)][OTf]_2$. Ellipsoids are shown at the 50% probability level. Hydrogen atoms, co-crystallized solvents and outer sphere counter ions are not shown for clarity.

Special Refinement Details for $[LFe_3(PhPz)_3OFe(NO)][OTf]_2$ (7). For the co-crystallized dichloromethane molecules similarity restraints were used to refine the 1,2 distances to be similar to one another. Enhanced rigid bond restraints were used on the triflate counter ions (S2 through C107) and all co-crystallized solvent molecules, while additional isotropic restraints were used on C102.

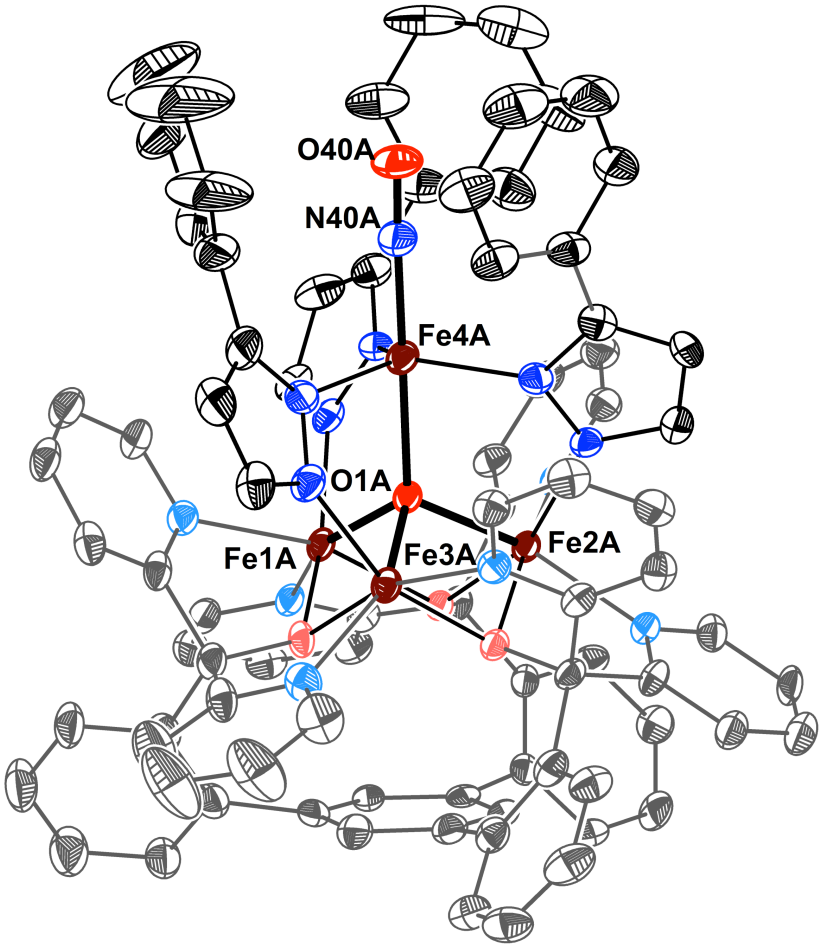

Figure S37. Crystal structure of $[LFe_3(PhPz)_3OFe(NO)][OTf]_3$. Ellipsoids are shown at the 50% probability level. Hydrogen atoms, co-crystallized solvents and outer sphere counter ions are not shown for clarity.

Special Refinement Details for $[LFe_3(PhPz)_3OFe(NO)][OTf]_3$ (8). The structure contains two molecules in the asymmetric unit, with a total of six triflate counter ions, of which four are disordered over several positions. The total number of triflates is fixed to six, to account for the charge balance. The first triflate counter ion is disordered over two positions refined with occupancies of 66.1% (S113 through C113) and 33.9% (S112 through C112). The second triflate is disordered over two positions, one of which is shared with a co-crystallized dichloromethane molecule. The triflates occupancies refined as 69.7% (S115 through C115) and 30.3% (S114 through C114), and the population of the DCM molecule was tied to that of the appropriate triflates ion (30.3%). The last two triflate counter ions are disordered over four different positions in close proximity, and refined with the following occupancies; 46.8% (S108 through C108), 31.3% (S109 through C109), 53.2% (S110 through C110), and 68.7% (S111 through C111). The single-site triflate counter ion (S106 through C106) was used to refine the 1,2 and 1,3 distances with similarity restraints on all the other triflate counter ions, while the single site dichloromethane molecule (C104 through Cl0A) was used to refine the 1,2 distance with similarity restraints on the disordered dichloromethane (C105 through Cl4). Enhanced rigid bond restraints were used on triflates counter ions (S110 through C110), (S111 through C111), (S114 through C114), the co-crystallized diethyl ether (O200 through C103) and both dichloromethane (C104 through Cl0A; C105 through Cl4) solvent molecules. Atoms C109 and S109 were set to have equivalent anisotropic displacement parameters.

Table S4. Selected spectroscopic, Mössbauer, and structural parameters for complexes **3** and **6**–**8** (entries 13–16), together with other mono-metallic trigonal bipyrimidal (TBP) Fe-complexes containing a single axial NO ligand.

Entry	Complex	Infrared	Mössbauer		X-ray Crystallograpy					Ref.
		$^{\nu}$NO (cm^{-1})	δ (mm/s)	$\lvert \Delta E_q \rvert$ (mm/s)	X-M (Å)	M-N (Å)	N-O (Å)	X-M-N (º)	M-N-O (º)	
1	$[NEt_4][Fe(N(CH_2CH_2S)_3)NO]$	1621	0.37	0.68	2.232(7)	1.721(8)	1.143(12)	179.0(4)	154.4(9)	1
2	$[NMe_4][Fe(N(o\text{-}CH_2PhS)_3NO]$	1639	-	-	2.178(4)	1.756(6)	1.11(3) 1.18(2)	176.3(2)	147.8(19) 145.9(16)	2
3	$[NMe_4][Fe(P(p\text{-}PhPhS)_3NO]$	1807	-	-	2.240(1)	1.676(3)	1.154(5)	177.72(12)	175.2(3)	2
4	$[PPN][Fe(P(p\text{-}SiMe_3\text{-}PhS)_3)NO]$	1720	-	-	2.210(1)	1.632(4)	1.259(9) 1.153(9)	174.48(17)	152.5(6) 162.8(7)	3
5	$K[Fe(N(CH_2CON\text{-}^{i}Pr)_3)NO]$	1729 1712	0.427	1.294	2.189(3)	1.735(4)	1.122(5)	179.2(2)	178.2(5)	4
6	$K[Fe(N(CH_2CON\text{-}cyp)_3)NO]$	1739 1712	0.412	1.336	2.184(4)	1.737(4)	1.138(5)	179.4(2)	172.7(4)	4
7	$K[Fe(N(CH_2CON\text{-}dmp)_3)NO]$	1750	0.430	1.331	2.198(2)	1.748(2)	1.146(3)	175.47(2)	160.3(2)	4
8	$K[Fe(N(CH_2CON\text{-}mbz)_3)NO]$	1760 1748 1731	-	-	2.205(5)	1.737(5)	1.150(6)	178.9(2)	175.6(5)	5
9	$[Fe(P(CH_2CH_2PPh_2)_3)NO][BPh_4]$	1690	-	-	2.225(3)	1.67(1)	1.16(1)	173.9(3)	177.4(7)	6
10	$[Fe(P(CH_2CH_2PPh_2)_3)NO][BPh_4]$	1700	-	-	2.15(8)	1.60(7)	1.19(9)	175.8 (3.8)	164(7)	7
11	$[Fe(TMG_3tren)NO)][OTf]_2$	1748	-	-	2.2502(18)	1.7479(19)	1.154(3)	179.24(8)	167.96(19)	8
12	$[Fe(afa^{cy})_3N][OTf]$	1744	-	-	-	-	-	-	-	9
13	$[LFe_3(PhPz)_3OFe][OTf]_2$	-	0.869	1.563	1.971(2)	-	-	-	-	this work
14	$[LFe_3(PhPz)_3OFe(NO)][OTf]_1$	1759 1723	0.592	2.381	1.968(2)	1.774(3)	1.157(3)	175.56(11)	169.6(3)	this work
15	$[LFe_3(PhPz)_3OFe(NO)][OTf]_2$	1796	0.550	2.271	2.035(3)	1.772(4)	1.144(5)	175.89(15)	171.4(4)	this work
16	$[LFe_3(PhPz)_3OFe(NO)][OTf]_3$	1823	0.617	1.937	2.087(5)	1.763(7)	1.144(8)	177.8(3)	171.9(7)	this work

Table S5. Crystal and refinement data for complexes **3**-**5**.

	Complex **3**	Complex **4**	Complex **5**
Empirical formula	$C_{92}H_{80}BF_4Fe_4N_{12}O_6$	$C_{96.73}H_{79.3}F_6Fe_4N_{15.16}O_{11}S_2$	$C_{90.1}H_{67.3}Cl_{1.78}F_9Fe_4N_{12}O_{13.55}S_3$
Formula weight (g/mol)	1759.89	2031.53	2088.54
T (K)	100.0	100.0	100.03
Radiation	CuKα (λ = 1.54178)	MoKα (λ = 0.71073)	MoKα (λ = 0.71073)
a (Å)	40.1338(10)	24.4372(11)	15.4560(7)
b (Å)	17.6952(4)	30.6281(15)	15.4962(7)
c (Å)	25.3732(6)	24.9731(12)	19.2923(10)
α (deg)	90	90	99.6189(19)
β (deg)	113.5582(13)	95.4328(15)	94.3724(19)
γ (deg)	90	90	93.4051(18)
V (Å^3)	16517.6(7)	18607.5(15)	4530.2(4)
Z	8	8	2
Cryst. syst.	monoclinic	monoclinic	triclinic
Space group	C2/c	C2/c	P-1
ρ_{calc}g (cm^3)	1.415	1.450	1.531
2 σ range (deg)	5.542 to 157.558	4.458 to 54.948	4.776 to 65.154
Crystal size/mm	0.21 × 0.04 × 0.01	0.2 × 0.08 × 0.04	0.21 × 0.18 × 0.15
μ (mm^{-1})	6.115	0.737	0.838
GOF	1.038	1.063	1.036
R1, wR2 (I> 2σ (I))	0.0701, 0.1655	0.0578, 0.1541	0.0740, 0.1981

Table S6. Crystal and refinement data for complexes **6**-**8**.

	Complex **6**	Complex **7**	Complex **8**
Empirical formula	$C_{91}H_{75}F_3Fe_4N_{13}O_{9.5}S$	$C_{91}H_{74}Cl_2F_6Fe_4N_{13}O_{13}S_2$	$C_{89.65}H_{66.31}Cl_{1.3}F_9Fe_4N_{13}O_{14.5}S_3$
Formula weight (g/mol)	1815.10	2030.05	2094.53
T (K)	100.0	100.05	100.05
Radiation	MoKα (λ = 0.71073)	MoKα (λ = 0.71073)	MoKα (λ = 0.71073)
a (Å)	12.1605(7)	23.0449(10)	17.9136(12)
b (Å)	29.0785(17)	16.4976(6)	20.5955(14)
c (Å)	22.8070(13)	24.0586(10)	26.4341(19)
α (deg)	90	90	76.679(2)
β (deg)	98.2302(17)	96.5282(13)	72.463(2)
γ (deg)	90	90	83.139(2)
V (Å^3)	7981.7(8)	9087.4(6)	9036.0(11)
Z	4	4	4
Cryst. syst.	monoclinic	monoclinic	triclinic
Space group	$P2_1/c$	$P2_1/c$	P-1
ρ_{calc}g (cm^3)	1.510	1.484	1.540
2 σ range (deg)	4.394 to 52.054	5.2 to 54.998	4.354 to 52.044
Crystal size/mm	0.22 × 0.04 × 0.03	0.2 × 0.2 × 0.1	0.17 × 0.17 × 0.06
μ (mm^{-1})	0.817	0.813	0.828
GOF	1.028	1.048	1.064
R1, wR2 (I> 2σ (I))	0.0506, 0.0995	0.0713, 0.2041	0.0976, 0.2571

References.

1. Davies, S. C.; Evans, D. J.; Hughes, D. L.; Konkol, M.; Richards, R. L.; Sanders, J. R.; Sobota, P. J. Chem. Soc. Dalton. Trans. **2002**, 2473.
2. Conradie, J.; Quarless, D. A.; Hsu, H.-F.; Harrop, T. C.; Lippard, S. J.; Koch, S. A.; Ghosh, A. *J. Am. Chem. Soc.* **2007**, *129*, 10446.
3. Lu, T.-T.; Chen, C.-C.; Liaw, W.-F. *Chem. Eur. J.* **2010**, *16*, 8088.
4. Ray, M.; Golombek, A. P.; Hendrich, M. P.; Yap, G. P. A.; Liable-Sands, L. M.; Rheingold, A. L.; Borovik, A. S. *Inorg. Chem.* **1999**, *38*, 3110.
5. Hammes, B. S.; Ramos-Maldonado, D.; Yap, G. P. A.; Liable-Sands, L.; Rheingold, A. L.; Young, V. G.; Borovik, A. S. *Inorg. Chem.* **1997**, *36*, 3210.
6. Di Vaira, M.; Tarli, M.; Stoppioni, P.; Sacconi, L. *Cryst. Struc. Commun*. **1975**, *4*, 653.
7. Di Vaira, M.; Ghilardi, C. A.; Sacconi, L. *Inorg. Chem*. **1976**, *56*, 1555.
8. Speelman, A. L.; Lehnert, N. *Angew. Chem. Int. Ed.* **2013**, *52*, 12283
9. Matson, E. M.; Park, Y. J.; Fout, A. R. *J. Am. Chem. Soc.* **2014**, *136*, 17398